NACA RM E54K01

NACA

RESEARCH MEMORANDUM

PRELIMINARY INVESTIGATION OF SOME INTERNAL BOUNDARY-LAYER-CONTROL SYSTEMS ON A SIDE INLET AT MACH NUMBER 2.96

By Thomas G. Piercy

Lewis Flight Propulsion Laboratory
Cleveland, Ohio

NATIONAL ADVISORY COMMITTEE FOR AERONAUTICS

WASHINGTON

February 18, 1955
Declassified December 3, 1958

NATIONAL ADVISORY COMMITTEE FOR AERONAUTICS

RESEARCH MEMORANDUM

PRELIMINARY INVESTIGATION OF SOME INTERNAL BOUNDARY-LAYER-CONTROL SYSTEMS ON A SIDE INLET AT MACH NUMBER 2.96

By Thomas G. Piercy

SUMMARY

An experimental investigation was performed at Mach number 2.96 to study the effects of some internal boundary-layer-control systems on the pressure recovery and stability characteristics of a side inlet employing half a double-shock external compression surface. External boundary-layer removal was provided with wedge diverter systems. Internal boundary-layer removal was obtained from porous bleed sections located at the inlet throat on the spike centerbody and on the floor of the inlet between the centerbody and the inlet cowl. Because of the geometry of the model, floor suction could be applied only for the case of zero external boundary-layer removal.

Centerbody bleed did not appreciably improve the performance of the inlet, and the maximum pressure recovery obtained was 62 percent. However, the total pressure was increased from 35 to 48 percent when the floor bleed system was used for the case of zero external boundary-layer removal.

Subcritical shock stability was not increased by the use of internal boundary-layer bleed. However, it was indicated that stability could be increased by the injection of high pressure air along the surface of the second compression cone, thereby adding energy to the cone boundary layer and decreasing its tendency to separate upon passing through the inlet terminal shock.

INTRODUCTION

A large portion of the total-pressure losses occurring in an air induction system at supersonic speeds is a result of viscous effects in the internal flow passages. The boundary layer, which builds up on the external compression surfaces of the inlet or enters because of insufficient external boundary-layer removal, may cause diffuser losses because of (1) the inherent low total pressure of the boundary-layer air,

or (2) interaction between the boundary layer and the main stream. This interaction may occur at the terminal shock and prevent location of that shock at its design position; separation at this point or farther inside the diffuser reduces the effectiveness of the subsonic diffuser and in addition may result in unsatisfactory velocity profiles at the diffuser exit.

A basic approach to minimize these internal losses is to utilize internal boundary-layer control. Internal boundary-layer-removal scoops and flush slots have been used successfully on a double-shock, external-compression, two-dimensional inlet in reference 1.

The main purpose of this report is to present the results of an experimental investigation on the effectiveness of porous internal bleed sections for a side inlet model at Mach number 2.96. The model chosen was a half-conical, double-shock inlet which was previously described in reference 2. The results of another study were used to locate the bleed surfaces; in reference 3 a tuft study of the internal flow of a half-conical side inlet with external boundary-layer removal revealed that boundary-layer separation occurred on the centerbody and also upon part of the inlet floor between the centerbody and the inlet cowl. Porous bleed sections were therefore located at the inlet throat on both the centerbody and the inlet floor.

Additional tests were conducted briefly to determine the effectiveness of flow injection along the surface of the second compression cone as a means of attaining subcritical shock stability.

These tests were conducted in the 18- by 18-inch Mach number 3.05 tunnel at the NACA Lewis laboratory.

SYMBOLS

The following symbols are used in this report:

A	area
d	wedge base dimension, 4.88 in.
h	boundary-layer-removal height
h/δ	dimensionless boundary-layer-removal parameter
l	distance from spike tip to wedge tip, 2.34 or 0 in.
l/d	wedge position parameter, dimensionless

m	mass flow, ρVA
m_3/m_0	mass-flow ratio, $\frac{\rho_3 V_3 A_3}{\rho_0 V_0 A_0}$
P	total pressure
p	static pressure
V	velocity
α_w	included angle of boundary-layer-removal wedge
δ	boundary-layer thickness 1/2 inch upstream of spike tip, distance from flat plate where velocity is equal to 0.99 free-stream velocity, 0.237 in.
ρ	density

Subscripts:

0	free stream
3	exit rake station (model station 28.0)
BL	bleed
g	spike gap
i	injected air

APPARATUS AND PROCEDURE

Model

The model for the present bleed tests was a half-conical, double-shock side inlet mounted on a flat plate; external boundary-layer removal was provided by means of wedge diverter systems. The present model has previously been described in reference 2 and incorporates the optimum features of the various configurations of that study: (1) a constant-area throat length of 2 inlet radii, (2) a boundary-layer splitter plate with leading edges swept from the spike tip to the inlet lip, and (3) two wedge diverter configurations; namely, a 30° wedge having an apex that coincided with the tip of the cone compression surface, and a 50° wedge having its apex located 2.34 inches downstream of the tip of the cone.

A schematic drawing of the model is presented in figure 1. The spike centerbody is characterized by a 2-inch constant-diameter section between model stations 0 and 2.0. Several porous bleed sections were installed in this constant-diameter section so as to vary both the amount and, to a limited extent, the location of the bleed surfaces. These bleed sections are indicated in figure 2, which presents a view of the spike centerbody and its components. In the constant-diameter region there were four alternative sections; (1) a 2-inch bleed section, (2) a 1-inch bleed section located rearward combined with a 1-inch nonporous or solid section located forward, (3) a 1-inch bleed section located in the forward position, and (4) a solid 2-inch insert.

Several bleed sections were also tested on the floor of the model between the centerbody and the inner cowl lip (see fig. 1), and a photograph of these is presented in figure 3. It is seen that again the location and amount of bleed surface could be varied. Each porous bleed section used herein was formed from Lektromesh screen of 40 count and 0.0075-inch thickness, and had 36 percent open area. This commercially available screen material is not woven but rather is a smooth, one-piece metal product formed by electrodeposition. No attempt was made to vary the porous surface during these tests.

Pertinent bleed-section areas are presented in the following table (duct area A_{BL} is the area of the duct at the exit of the bleed manifolds):

Bleed section	Total area of bleed surface, sq in.	Open area of bleed surface, sq in.	Duct area A_{BL}, sq in.
Full centerbody	7.23	2.60	0.61
Partial centerbody	3.61	1.30	.61
Full floor	2.20	.79	.61
Partial floor	1.22	.44	.61

Bleed air was taken through holes in the main plate and was collected with the two separate manifolds of figure 4, from which it was ducted out of the tunnel. Rotameters were used in each bleed duct to measure and control the rate of bleed flow. Bleed air was then returned to the tunnel test section.

Limited tests were also run with the two-piece spike tip of figure 5. This component was so formed that first and second cone compression surfaces were separated by a maximum gap of 0.06 inch; with this gap, the over-all length was the same as that of the original spike tip. The compression shock pattern at the inlet lip could be altered by moving the forward piece with respect to the second compression surface. This cone tip was also used when high-pressure air ducted from the atmosphere was

injected along the second compression cone surface in an attempt to energize the cone boundary layer and reduce the tendency toward separation, thus promoting subcritical shock stability.

Photographs of the model mounted in the tunnel are presented in figure 6. Figure 6(a) represents the configuration for no external boundary-layer removal, while figure 6(b) corresponds to full external boundary-layer removal ($h/\delta \geq 1.0$) provided by a 50° included angle wedge. The bleed air ducting is evident in these photographs.

Instrumentation

Total-pressure recovery was obtained from the area-weighted readings of a 41-tube rake located at the diffuser exit. Inlet mass flow was determined using this total-pressure recovery together with the assumption of a choked exit, the area of which was controlled with a remotely operated exit plug. This instrumentation is identical to that described in reference 2.

Additional instrumentation included static orifices located every 1/2 inch on the surface of the inner cowl lip to aid in positioning the internal normal shock of the inlet. Static orifices were located in the ducting of each bleed system, the injection system, and the outlet of the rotameters.

Pertinent areas of the injection system are presented in the following table (the reference area A_i is the area of the duct immediately ahead of the gap and is the station at which the static pressure of the injected air was measured):

Spike gap, in.	A_i, sq in.	A_g/A_i
0.025	0.149	0.347
.015	.149	.207
.010	.149	.139

Unstable operation of the inlet was observed with schlieren equipment and was measured with dynamic pressure pickups that operated pen-type recorders.

DISCUSSION OF RESULTS

Inlet Performance with Internal Bleed

Presented in figure 7 is a typical diagram of inlet performance with internal bleed. With no bleed flow, little or no subcritical stability was obtained; that is, shock instability occurred for inlet mass-flow ratios lower than that corresponding to the maximum or supercritical value. With the maximum possible bleed-flow rate (determined by the available pressure ratios when the rotameter outlet valve was completely open), the performance curve was shifted to the left, indicating a reduction in mass flow discharged from the subsonic diffuser. Generally this reduction of inlet mass flow was not the result of stable subcritical shock spillage, but rather represented the amount of bleed flow. The amount of bleed flow was approximately constant when the inlet normal-shock system was downstream of the porous bleed surface. However, at the higher inlet total-pressure recoveries, the normal shock moved onto the porous bleed surface and the bleed flow generally increased, as indicated in figure 7.

The intermediate performance curves correspond to less than maximum possible bleed flow and were determined in these tests for fixed values of the rotameter outlet pressure. A peak pressure recovery, indicated by the triangles, was obtained for each intermediate bleed rate; for inlet back pressures greater than those corresponding to the peak pressure recovery, inlet instability occurred. Some improvement of the maximum pressure recovery was generally obtained by the bleeding action, indicating a reduction of the internal diffuser losses over the case without bleed flow.

Data presented in this report are for operation without bleed flow, for maximum bleed flow operation, and the envelope of the maximum pressure recoveries at the intermediate bleed rates. The supercritical intermediate bleed flow curves are not presented, since the rotameter outlet pressures used herein have no significance for an actual installation which would use a different throttling system. However, the throttling pressure ratios necessary to obtain these bleed rates are discussed.

Inlet performance with no external boundary-layer removal (h/δ, 0) and no bleed flow is presented in figure 8. These data were obtained with the solid or nonporous inserts in both centerbody and floor bleed sections. This performance is to be compared with that obtained with internal bleed in figures 9 and 10; figure 9 corresponds to several centerbody bleed arrangements, while figure 10 corresponds to combinations of both floor and centerbody bleed.

It is indicated in figure 9 that each bleed configuration offered an improvement in total-pressure recovery ratio of 0.02 to 0.03 over the corresponding no-bleed-flow case. It is further noted that both inlet pressure recovery and mass flow were affected by the insertion of bleed sections even when no air was bled; a comparison of the no-bleed-flow cases of figure 9 with that of figure 8 indicates that the insertion of bleed sections reduced the captured inlet mass-flow ratio by as much as 0.04, while total-pressure-recovery ratio increased by only about 0.02.

The same effect on inlet performance was obtained when a 1-inch strip of number 100 carborundum dust was put on the centerbody to simulate the roughness of the bleed section. Hence, for the case of zero external boundary-layer removal, the changes in performance noted with insertion on the bleed surfaces were probably due only to the roughness of these surfaces.

In figure 10, for various combinations of floor and centerbody bleed sections at h/δ of 0, it is observed that bleeding through the floor sections in combination with the centerbody yielded higher pressure recoveries than were obtained with centerbody bleed alone. However, by eliminating centerbody bleed flow entirely and using only the floor bleed, even further improvements in inlet total pressure were realized. A maximum pressure recovery of 48 percent was obtained using the full floor bleed configuration, representing a 37 percent increase over the original no-bleed case. It is indicated that boundary-layer accumulation in the corners of half-conical inlets is very detrimental to subsonic diffuser pressure recovery.

While it is likely that further improvements could have been realized with floor bleed sections extending farther downstream into the diffuser, it is very doubtful that the pressure recovery could have been increased to that obtained with external boundary-layer removal ahead of the inlet (i.e., about 62 percent). It is noted in figures 9 and 10 (and in subsequent bleed performance figures) that the bleed mass flow did not vary in proportion to the amount of bleed surface area. While this effect is not completely understood, the possibility of choking in the bleed ducting may be definitely dismissed inasmuch as the Mach number in the minimum area sections of the ducting rarely exceeded 0.4.

Figures 11 and 12 present inlet performance data with several internal centerbody bleed arrangements for various amounts of external boundary-layer removal provided by 30° wedges in the forward position (l/d, 0) and 50° wedges in the rearward position (l/d, 0.48), respectively. Suction on the floor of the model was not attempted for the cases of external boundary-layer removal ($h/\delta > 0$); with the wedge-type boundary-layer-removal configurations, bleeding from the floor would have required ducting between the inlet floor and the main boundary-layer plate which would have obstructed the wedge removal surface. Inlet performance with

internal centerbody bleed for each external boundary-layer-removal configuration is compared with the no-bleed case obtained when the solid or nonporous centerbody insert was used.

For the 30° wedge removal configuration of figure 11, it is noted that the insertion of bleed surfaces generally lowered the no-bleed-flow performance, particularly at the higher values of h/δ. While internal bleed improved the diffuser recovery over the no-bleed-flow case, the peak pressure recovery never exceeded the original performance. In contrast to the results previously noted for the case of no external boundary-layer removal, the reduction of pressure recovery by insertion of bleed surfaces was not directly attributable to the roughness caused by the porous bleed section, inasmuch as the addition of a strip of roughness to the original model did not affect the performance. The loss of pressure recovery is more likely due to the effective abrupt change in flow area distribution caused by the volume of the plenum chamber beneath the porous bleed section and the consequent possibility that recirculation of air through the bleed surface interferes with the positioning of the terminal shock. Inasmuch as the centerbody bleed configurations did not substantially improve the over-all inlet pressure recovery, the potential usefulness of the centerbody bleed configurations is probably restricted to that of serving as a bypass for engine-inlet matching; it is noted that such a bypass would generally maintain or improve the diffuser pressure level.

It was indicated previously in figure 10 that the pressure recovery gains using centerbody bleed were relatively poor in comparison with that which could be obtained using floor bleed at h/δ of 0. It is likely that floor bleed (or removal of the boundary layer in the corners of the inlet with an internal scoop) would also have been more effective than centerbody bleed when combined with external boundary-layer removal ahead of the inlet.

The data of figure 12 for the 50° wedge removal system indicate essentially the same results as were noted for the 30° wedge configurations and therefore will not be discussed. In an attempt to improve the inlet stability characteristics, one additional configuration was tested. The spike tip was perforated with a series of 48 holes of 0.041-inch diameter (see fig. 2) in the region of the inlet lip. These holes were then connected to the forward centerbody bleed section so that suction could be applied to the forward sections of the spike as well as in the constant-area throat region. This configuration did not improve the subcritical stability nor diffuser performance, although slightly more flow was bled than with the bleed section alone.

The total-pressure recovery of the bleed air is presented in figure 13. These results were obtained from continuity relations using the known bleed mass flow and the static pressure at the manifold sections. In

figure 13(a) for the centerbody-bleed configurations, the variation of bleed pressure recovery with h/δ for the two types of wedge removal followed the variations in total pressure of the main duct, although at a lower level. (For example, it will be noted that for the 50° wedge configuration, the maximum pressure recovery of both the main duct and the bleed occurred at h/δ of 0.793.) These losses are to be expected inasmuch as loss of total pressure would occur across the porous screen and also because the lower energy air of the main duct flow was removed. The data of figure 13(a) were obtained for the forward bleed sections but are quite representative inasmuch as only small variations with location of bleed section occurred with centerbody bleed. The data of figure 13(b) for the floor-bleed sections indicate that a variation of recovery was observed with location of bleed surface. It is observed that lower pressure recoveries were obtained with the rearward and full-bleed sections, indicating that lower energy air was being removed and thereby offering an explanation for the better inlet performance noted with these bleed sections. It is also observed that the floor bleed pressure recovery was lower than had been obtained with centerbody bleed at h/δ of zero, perhaps explaining the higher diffuser pressure recovery obtained using floor bleed.

CT-2

The total pressures of the bleed flow of figure 13 may be considered equivalent to the static pressure in the bleed ducting inasmuch as the flow was of low velocity. In an actual installation the amount of throttling of the bleed flow necessary to produce the peak pressure recoveries given herein may be obtained in the following manner: The bleed mass-flow ratio m_{BL}/m_0 may be obtained by subtracting the inlet mass-flow ratio at the desired operating point from the supercritical inlet mass-flow ratio with no bleed flow. Figure 13(a) or (b), depending upon the bleed configuration, may then be used to estimate the static pressure in the bleed ducting for this value of bleed mass flow.

Inlet Performance with Flow Injection on External Compression Surface

A limited investigation of inlet performance was obtained with the two-piece spike tip of figure 5. This phase of the study was initiated under the assumption that one of the possible causes of inlet buzz was the inherent inability of boundary layer on the conical compression surface to remain attached upon passing through the terminal shock structure of the inlet. With the two-piece spike tip, it was possible to inject high-pressure air (ducted from the atmosphere) along the surface of the second compression cone. The injection system was designed to add energy to the boundary layer and therefore to decrease its tendency toward separation upon passing through the inlet terminal shock.

Inlet performance data with flow injection are presented in figure 14 for several values of external boundary-layer-removal parameter h/δ.

For these tests the forward centerbody bleed section was installed but no flow was bled. The spike gap was varied in steps for each value of h/δ, and the data reported correspond to those spike gaps for which the lowest value of stable mass flow was attained. These spike gaps were 0.010, 0.015, and 0.025 inch for values of h/δ of 1.055, 0.793, and 0.262, respectively. Injection data presented correspond to the maximum flow injection rate (obtained when the throttling valve was completely opened) and to a smaller injection rate defined as the minimum injection rate with which stable operation could be maintained.

The data of figure 14 indicate that the use of flow injection was somewhat successful in delaying the onset of inlet buzz. Stable subcritical mass-flow spillages of 24, 17.5, and 49 percent of the critical mass flows were obtained at values of h/δ of 1.055, 0.793, and 0.262, respectively. Typical shadowgraphs of the flow in the region of the inlet are presented in figure 15 for the injection configuration. Photographs presented correspond to supercritical inlet operation with no flow injection and to stable subcritical operating with injection.

An examination of the injection configuration pressure recovery data of figure 14 indicates that while little or no loss in maximum pressure recovery was incurred when injection was applied, the maximum pressure recovery levels for the injection configurations are considerably lower than those obtained with the original spike tip of figure 11. Specifically, the injection configurations suffered total-pressure-ratio losses of approximately 0.040, 0.010, and 0.002 at values of h/δ of 1.055, 0.793, and 0.262, respectively, in comparison with the original spike tip configurations having forward centerbody-bleed surfaces and zero bleed flow. This effect is probably a function of the location of the compression surface oblique shocks relative to the inlet face.

An example of the effects of inlet shock location is indicated in figure 16. Presented is the performance obtained with the inlet at h/δ of 1.287 with 50° wedge removal. The forward centerbody bleed section was in the inlet throat but no flow was bled. Compared are data for the original spike tip and the two-piece spike tip with gap fully closed. With the original spike tip, both first and second oblique shocks passed just upstream of the inlet lip. Closing the spike gap allowed the first oblique shock to come closer to the inlet lip, while the second oblique shock apparently fell just inside the inlet lip. While the inlet mass-flow ratio increased slightly when the gap was closed, the critical total-pressure recovery decreased almost 0.070. The losses of critical total-pressure recovery previously cited for figure 14 were not so large as 0.070, presumably because of the more favorable shock configuration associated with the larger spike gaps.

Similar effects of inlet shock location were noted in reference 4 for a single-shock, conical-nose inlet, although the reduction of pressure recovery was not so large as observed herein.

The ratio of the static pressure of the injected air (measured just before it entered the spike gap) to free-stream static is presented in figure 17. Also given are the theoretical values of the static-pressure ratio on the second compression cone and behind the terminal shock of the inlet. It is noted that while the measured injection pressures exceeded those on the second cone, it was not necessary that the injected flow static pressure equal the pressure behind the normal shock for stabilization to occur.

On the basis of these pressure ratios and the area ratios presented earlier, it is evident that the gap exit was choked, at least for maximum injection. For these conditions the injection mass-flow ratios based on inlet capture area were 4.2, 2.8, and 2.2 percent for h/δ values of 0.262, 0.793, and 1.055, respectively.

In an actual turbojet installation neither internal bleed nor a scoop (in the regions considered) could provide the maximum injection pressure ratios presented in figure 17. For example, 90 percent total-pressure recovery would be required to give the pressure ratio corresponding to the maximum injection rate for h/δ of 1.055. However, the use of compressor bleed or an auxilliary pump could raise the pressure level to the desired range and pass the small amount of air required. Inlet total-pressure recovery with injection might be maintained at a high level by keeping the compression shocks from falling within the inlet.

CT-2 back

SUMMARY OF RESULTS

An experimental investigation to study the effects of various methods of boundary-layer control on the pressure-recovery, mass-flow, and stability characteristics of a half-conical, double-shock, external-compression side inlet at Mach number 2.96 yielded the following results:

1. Inlet total-pressure recovery was increased as much as 37 percent by the use of floor bleed for the case of zero external boundary-layer removal. Nevertheless, the increased pressure-recovery performance obtained with floor bleed (0.48) was still considerably lower than that obtained with external boundary-layer removal (0.62).

2. Bleeding from the centerbody did not appreciably improve the overall inlet pressure recovery.

3. Subcritical stability was increased when high-pressure air was injected along the surface of the second compression cone. It was indicated that compressor bleed air or an auxilliary pump could provide the necessary pressure and mass-flow ratios.

Lewis Flight Propulsion Laboratory
National Advisory Committee for Aeronautics
Cleveland, Ohio, November 17, 1954

REFERENCES

1. Obery, Leonard J., and Cubbison, Robert W.: Effectiveness of Boundary-Layer Removal Near Throat of Ramp-Type Side Inlet at Free-Stream Mach Number of 2.0. NACA RM E54I14, 1954.

2. Johnson, Harry W., and Piercy, Thomas G.: Effect of Wedge-Type Boundary-Layer Diverters on Performance of Half-Conical Side Inlets at Mach Number 2.96. NACA RM E54E20, 1954.

3. Piercy, Thomas G., and Johnson, Harry W.: A Comparison of Several Systems of Boundary-Layer Removal Ahead of a Typical Conical External-Compression Side Inlet at Mach Numbers of 1.88 and 2.93. NACA RM E53F16, 1953.

4. Beheim, Milton A.: A Preliminary Investigation at Mach Number 1.91 of a Diffuser Employing a Pivoted Cone to Improve Operation at Angle of Attack. NACA RM E53I30, 1953.

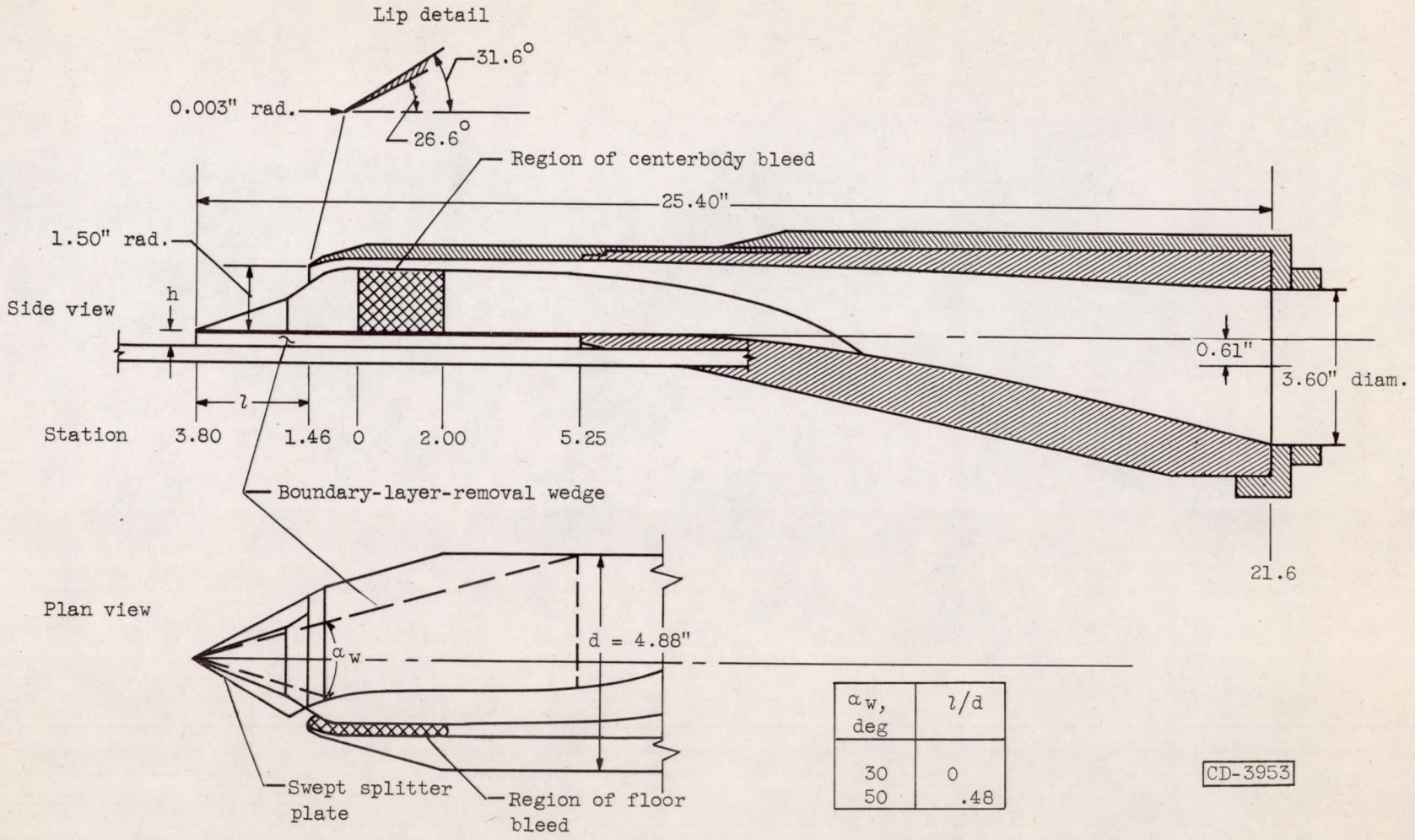

α_w, deg	l/d
30	0
50	.48

Figure 1. - Schematic diagram of model.

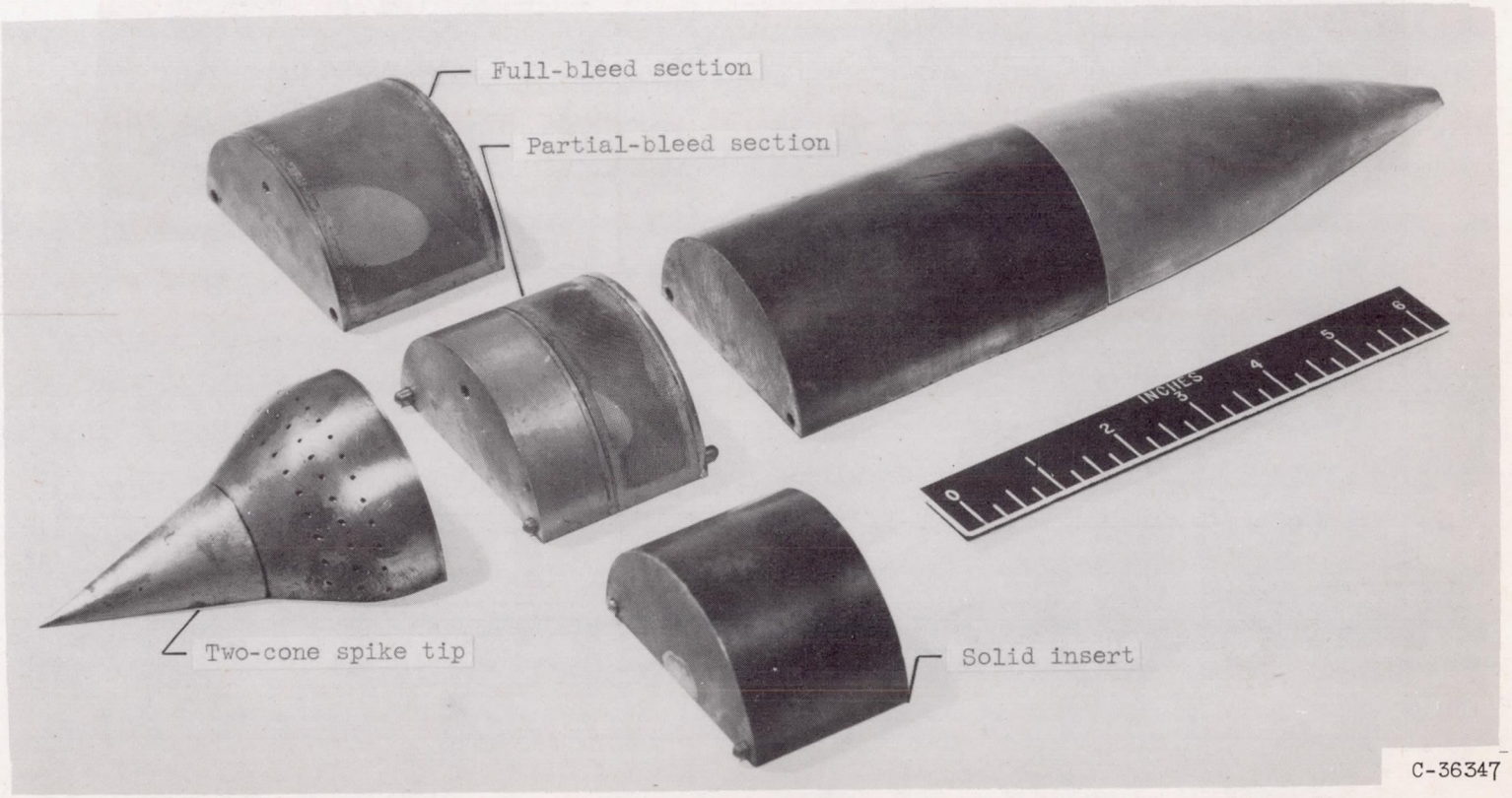

Figure 2. - Centerbody and component parts.

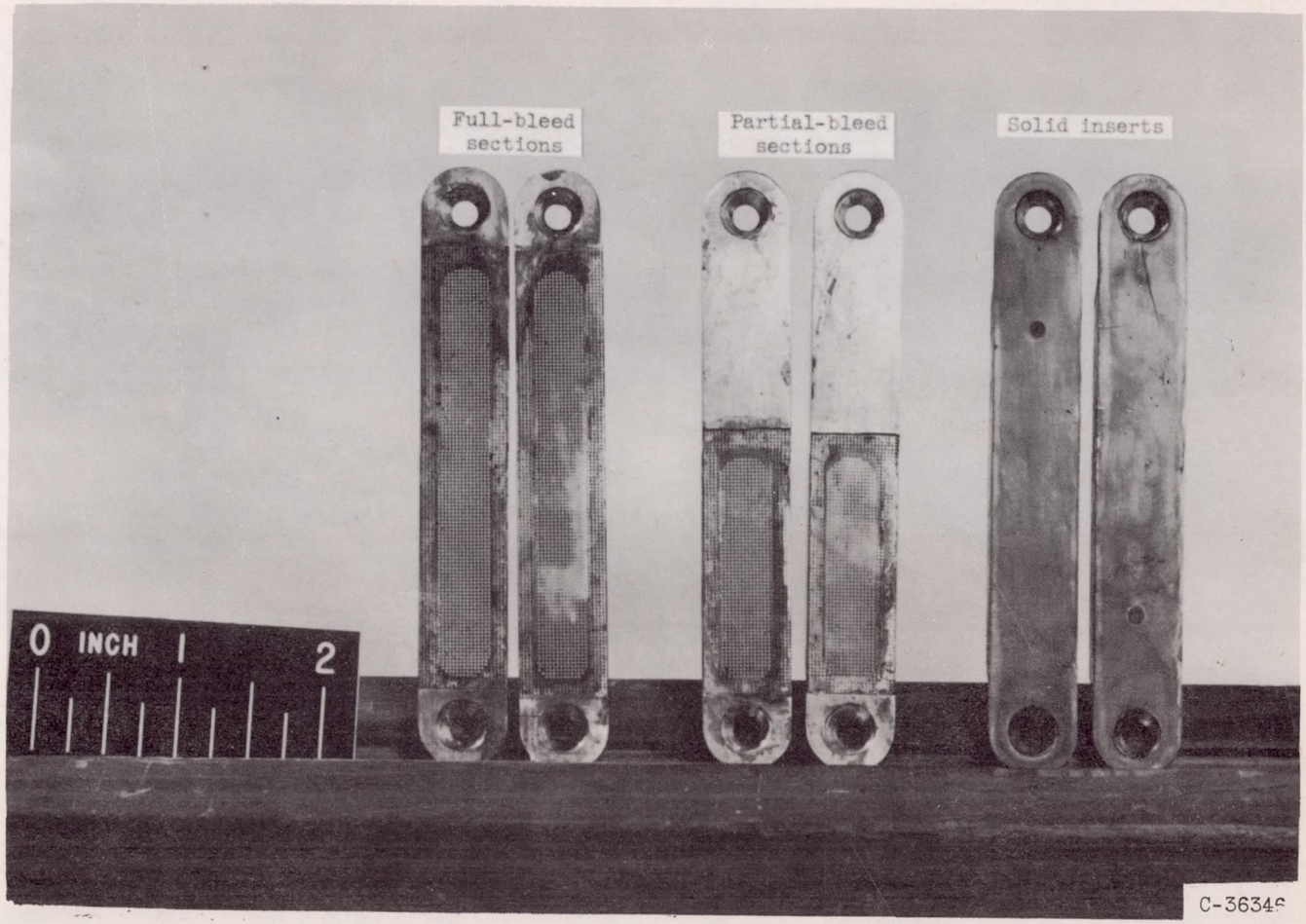

Figure 3. - Floor bleed sections.

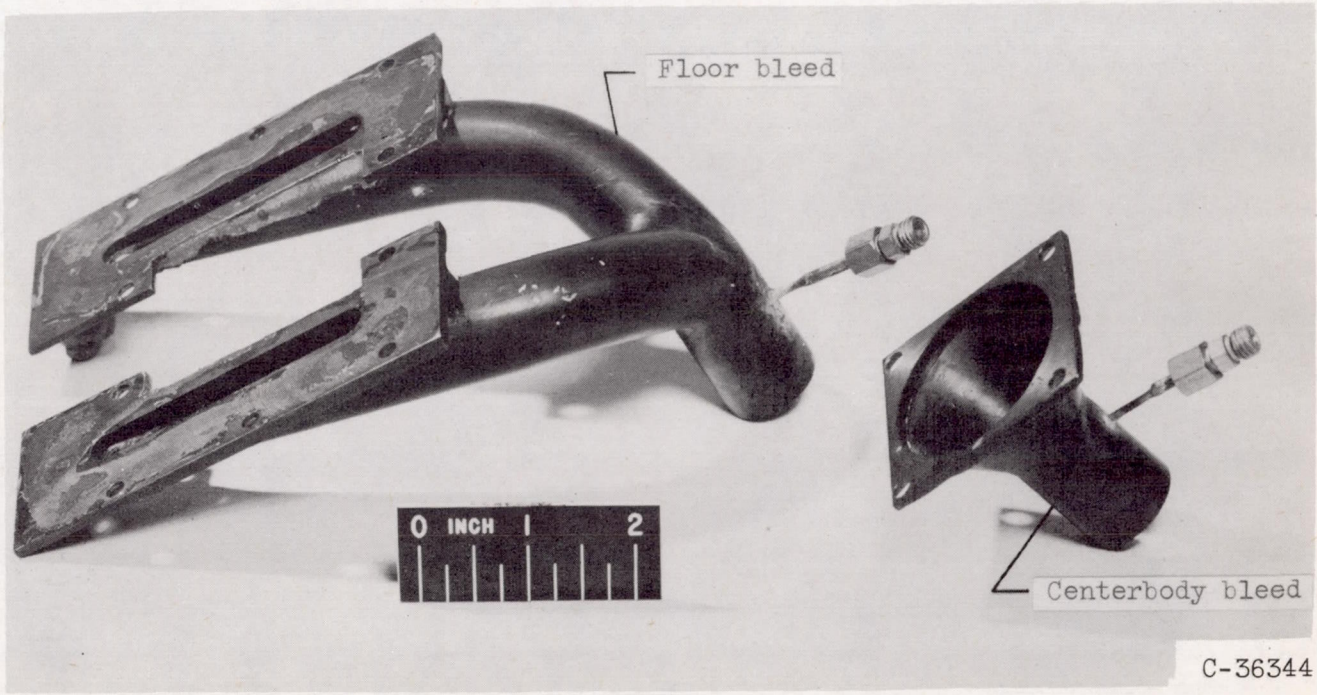

Figure 4. - Bleed manifolds.

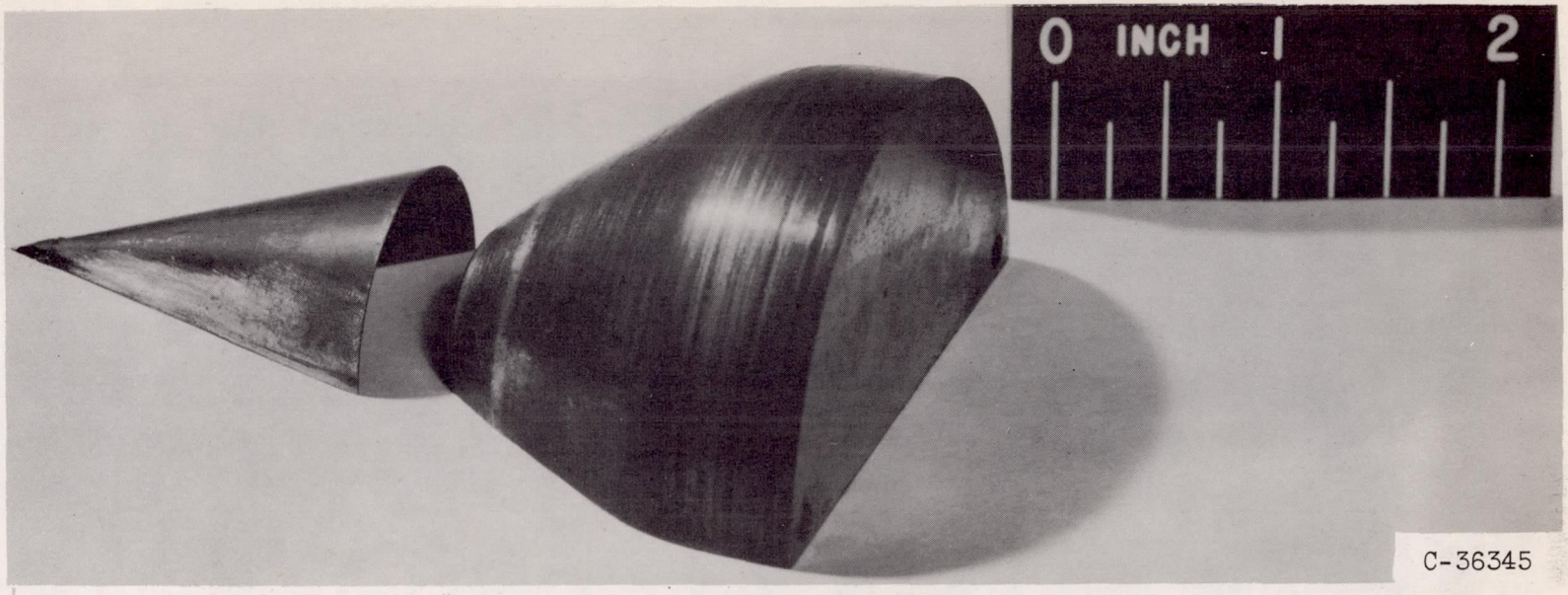

(a) Two-piece spike tip.

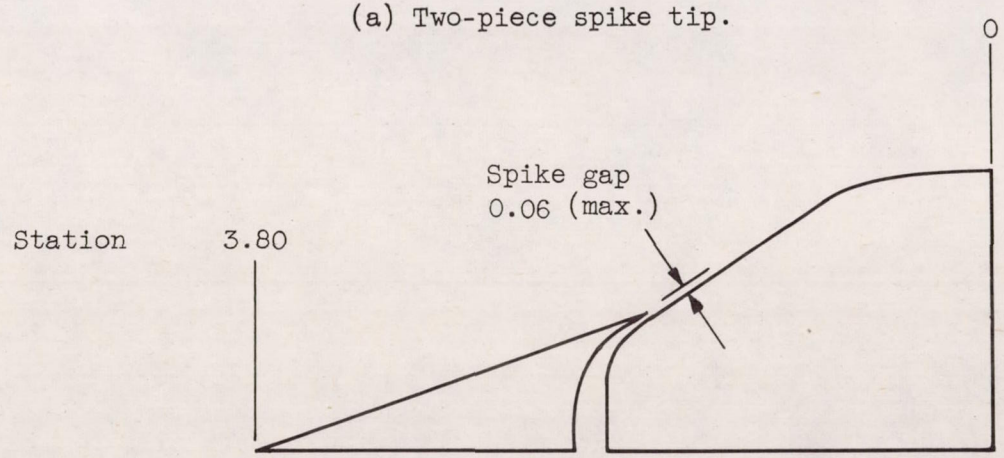

(b) Cross section of two-piece spike tip.

Figure 5. - Photograph and schematic drawing of two-piece spike tip.

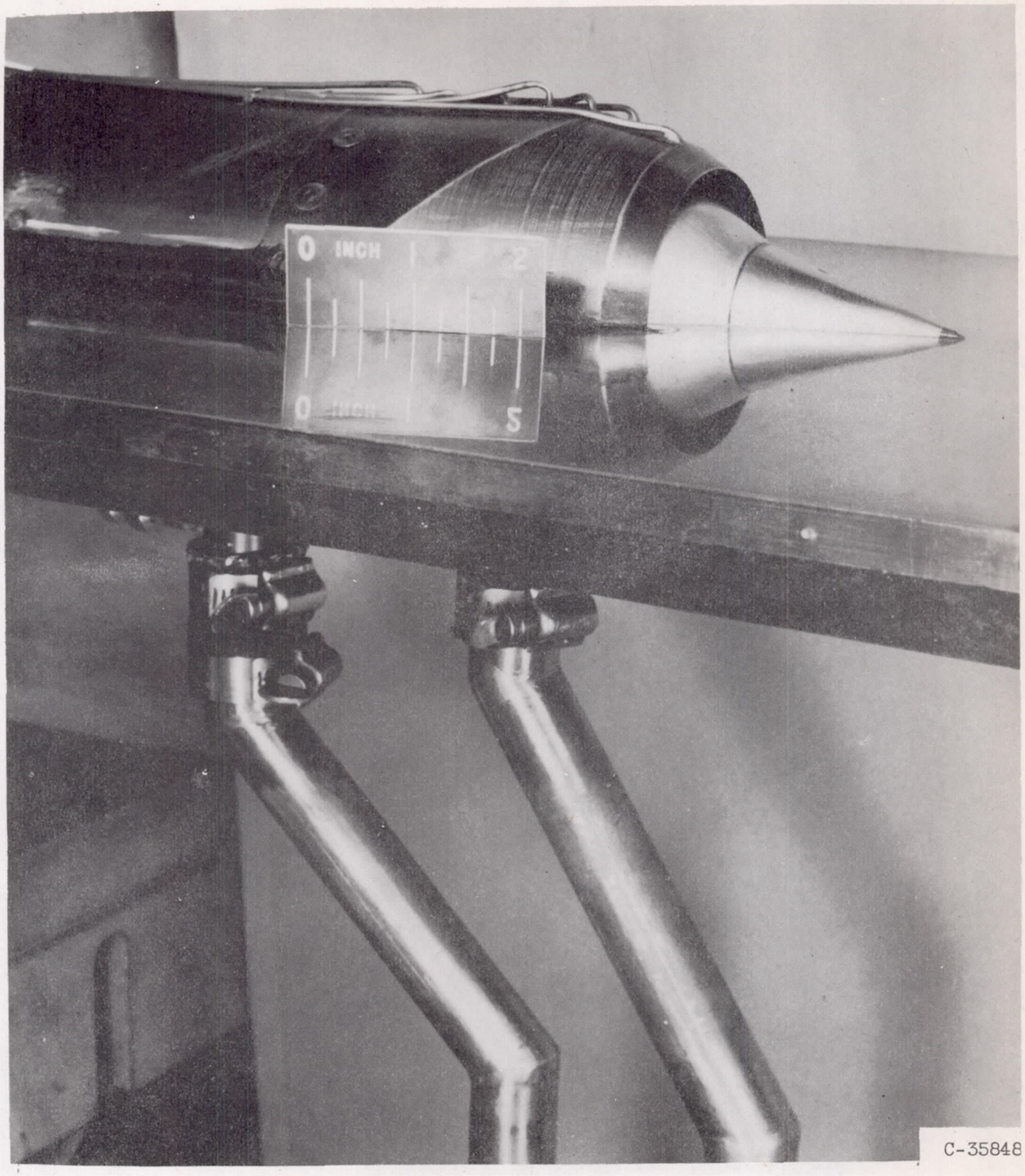

(a) No external boundary-layer removal.

Figure 6. - Photographs of model.

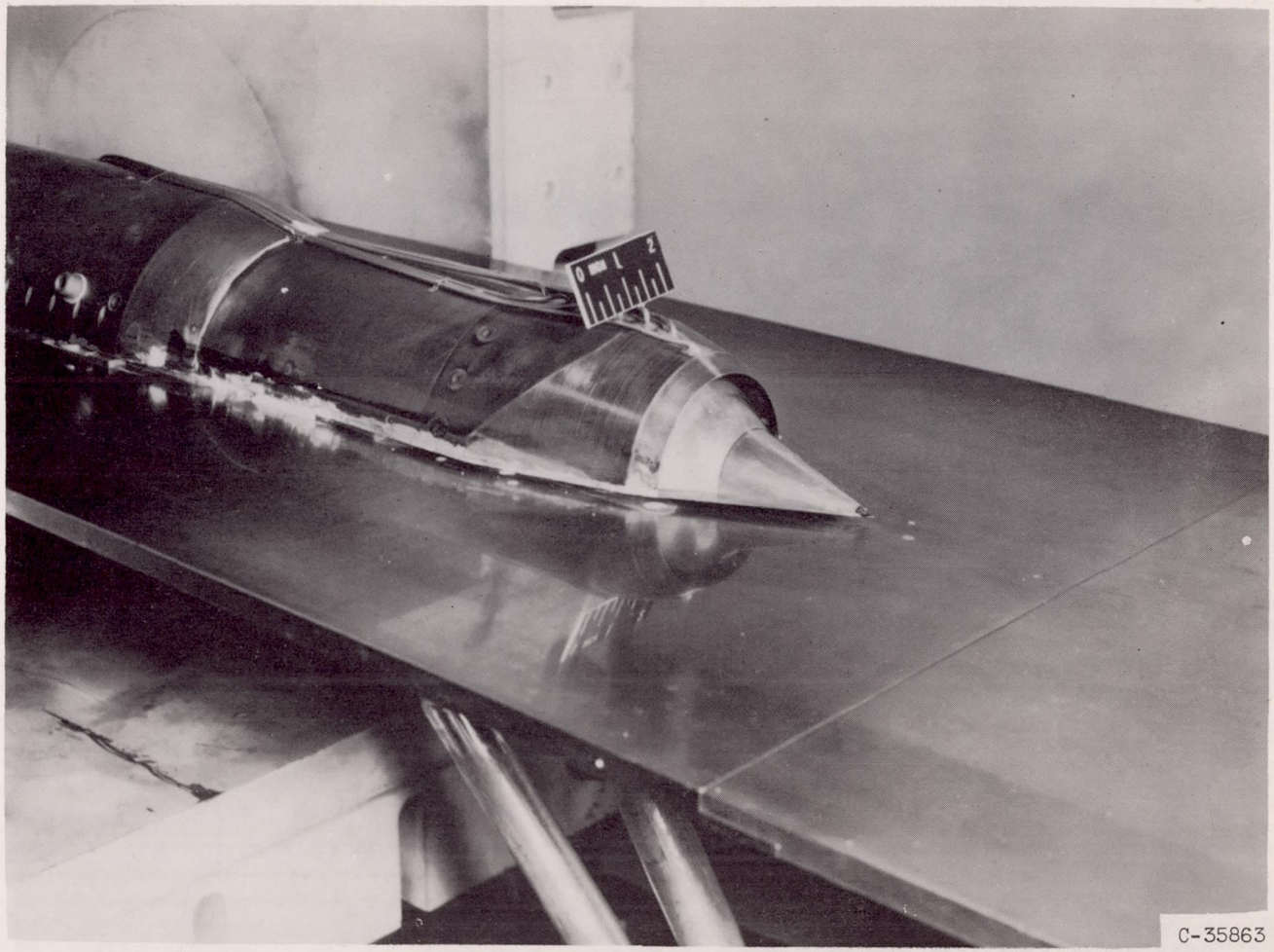

(b) 50° wedge external boundary-layer removal.

Figure 6. - Concluded. Photographs of model.

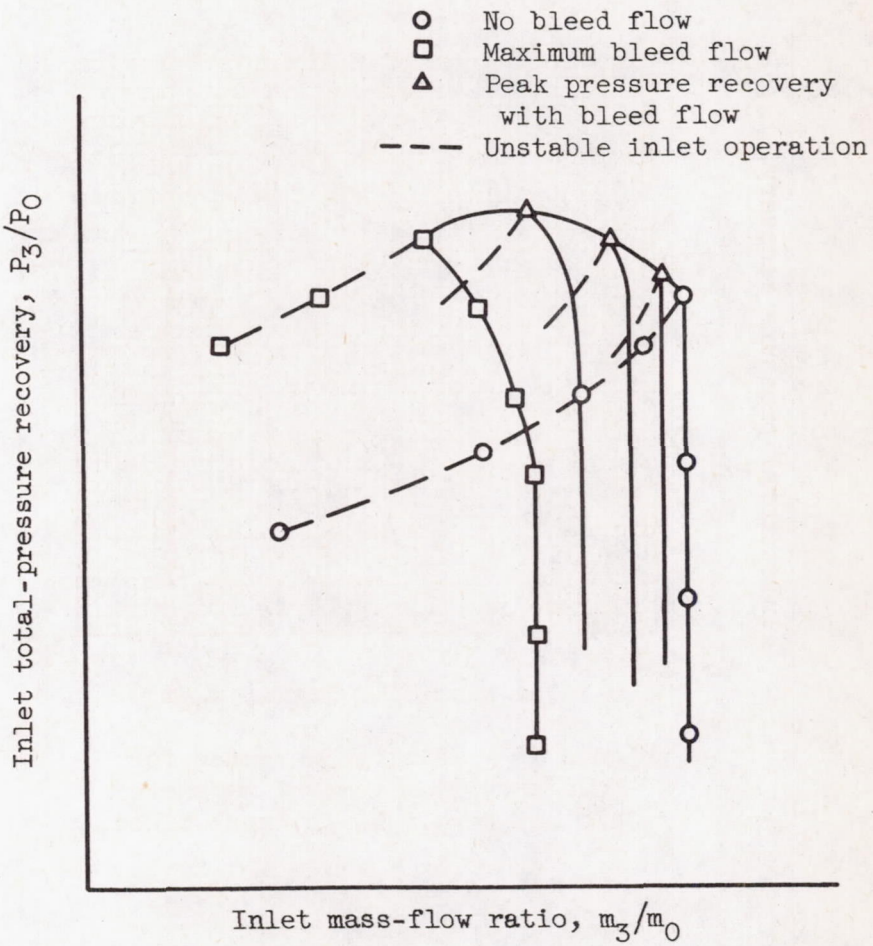

Figure 7. - Typical bleed flow performance diagram.

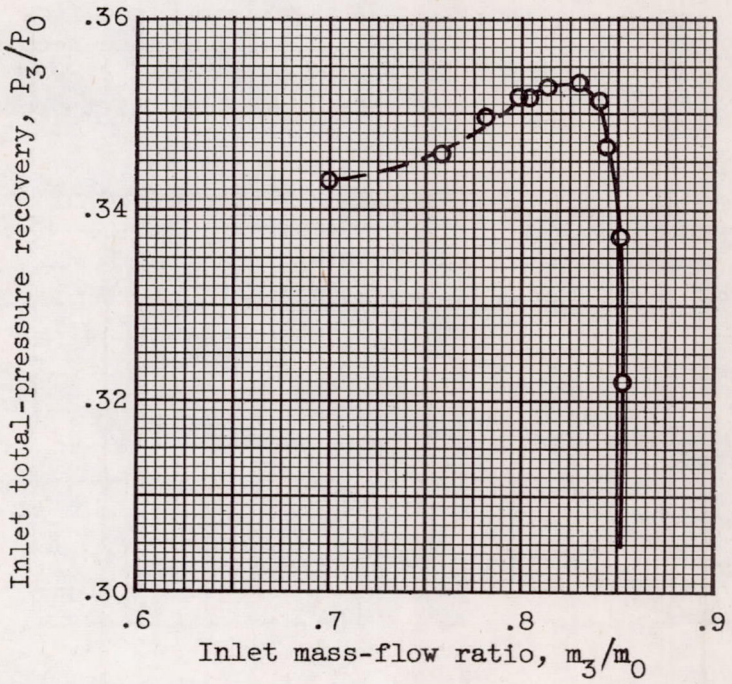

Figure 8. - Inlet performance for boundary-layer removal parameter h/δ of zero. No internal bleed.

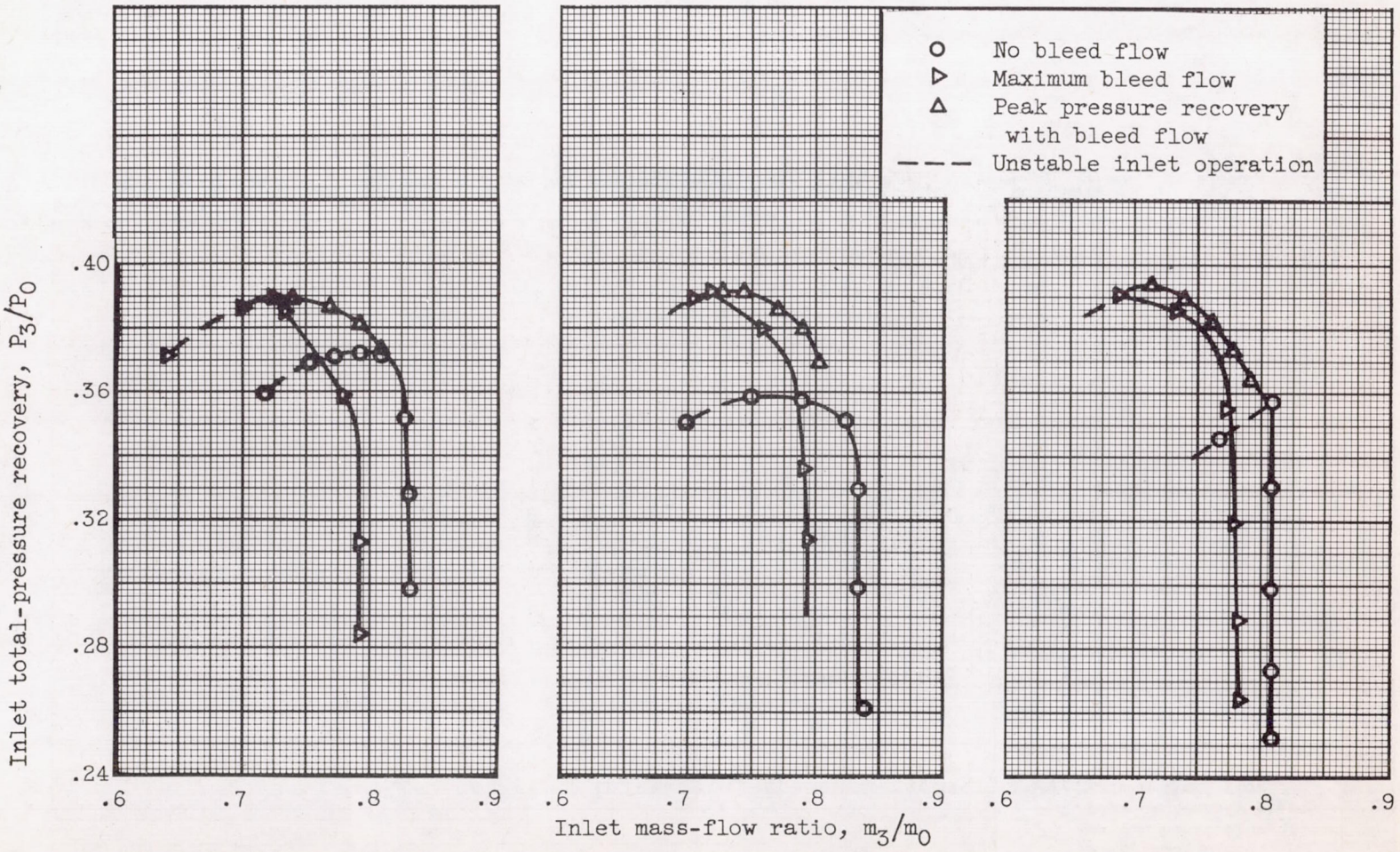

(a) Rearward bleed section (b) Forward bleed section. (c) Full-bleed section.

Figure 9. - Inlet performance with several centerbody bleed sections. Boundary-layer-removal parameter, h/δ, 0.

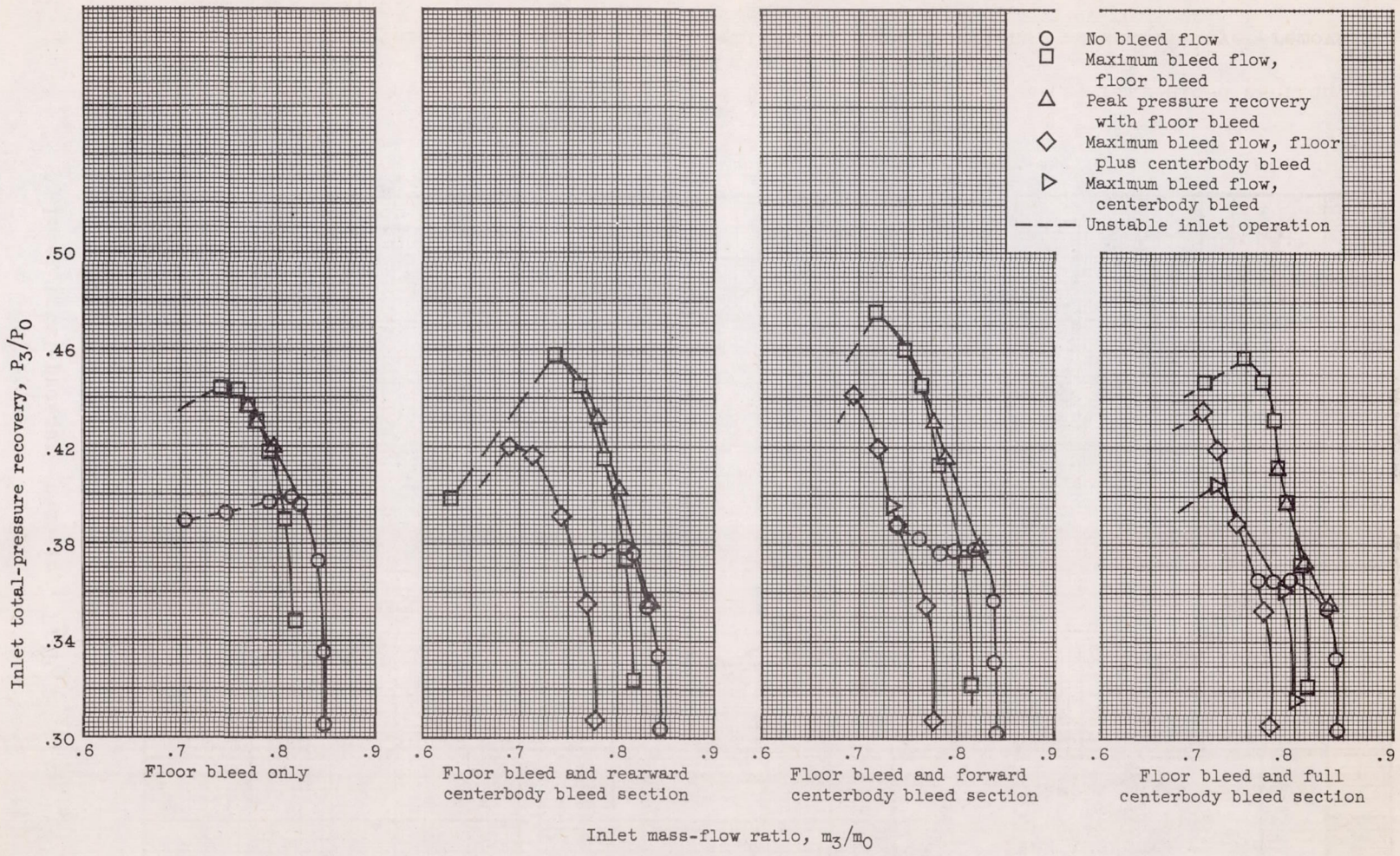

(a) Rearward floor bleed section.

Figure 10. - Inlet performance with several combinations of floor and centerbody bleed sections. Boundary-layer-removal parameter, h/δ, 0.

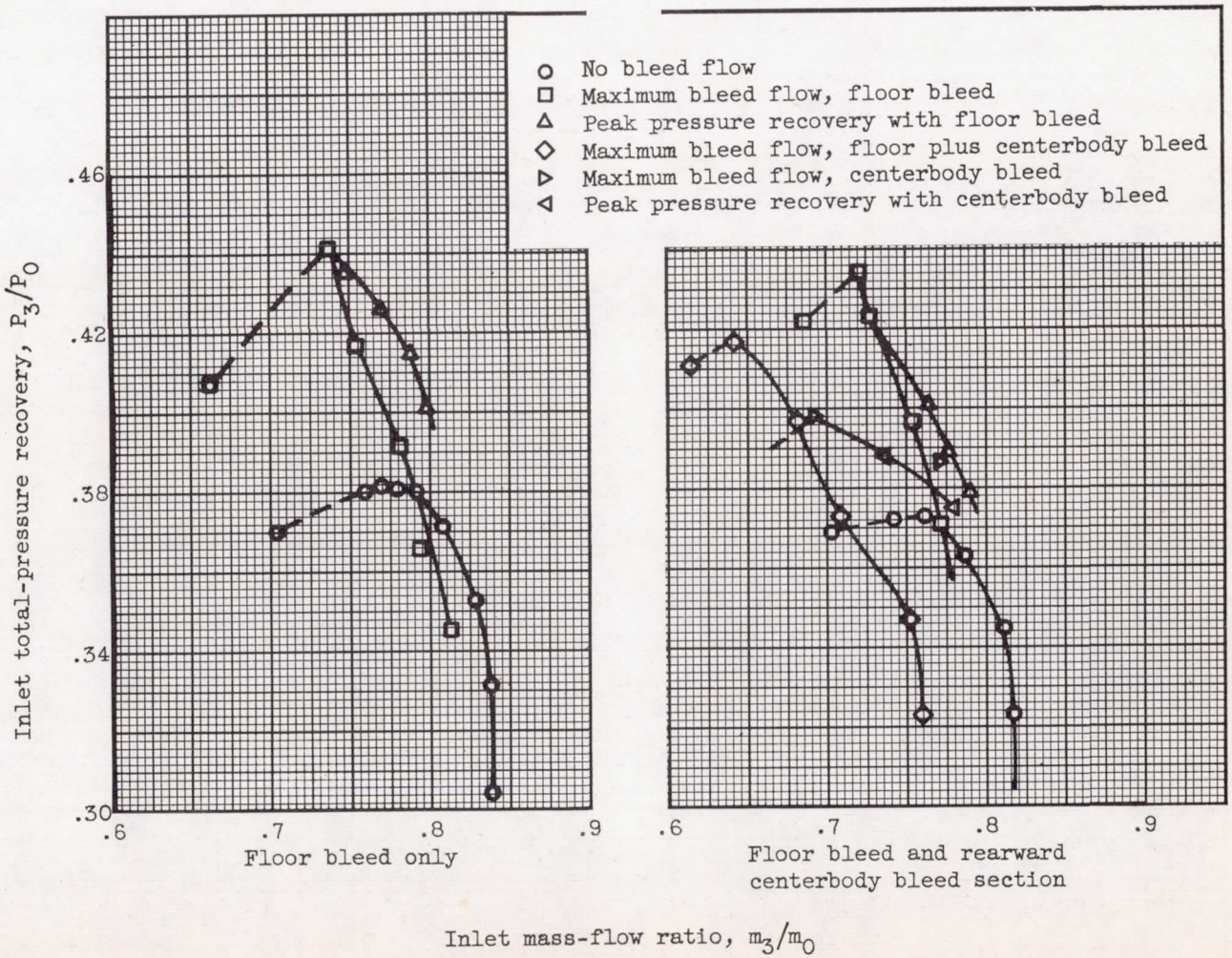

(b) Forward floor bleed section.

Figure 10. - Continued. Inlet performance with several combinations of floor and centerbody bleed sections. Boundary-layer-removal parameter, h/δ, 0.

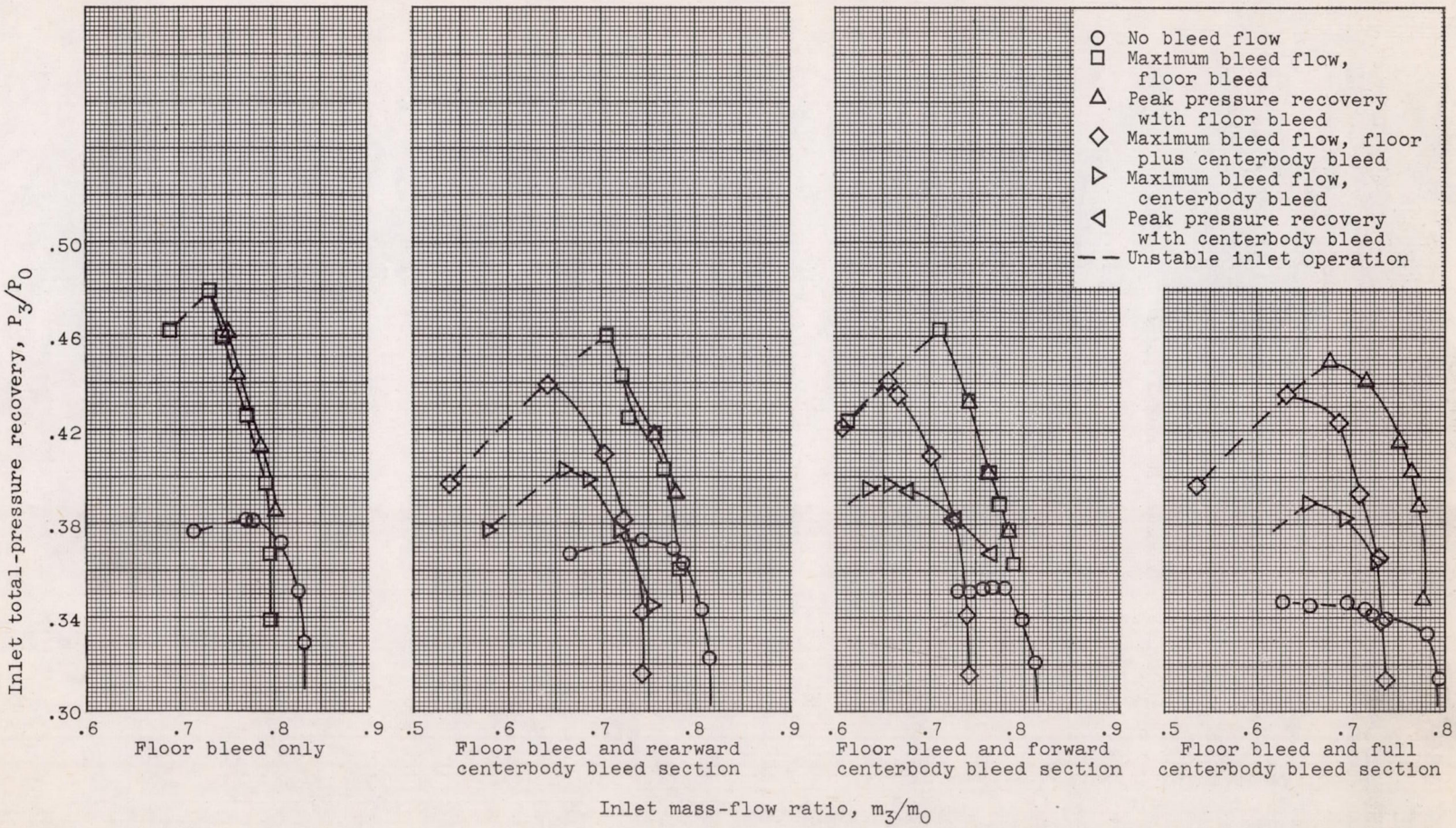

(c) Floor full bleed.

Figure 10. - Concluded. Inlet performance with several combinations of floor and centerbody bleed sections. Boundary-layer-removal parameter, h/δ, 0.

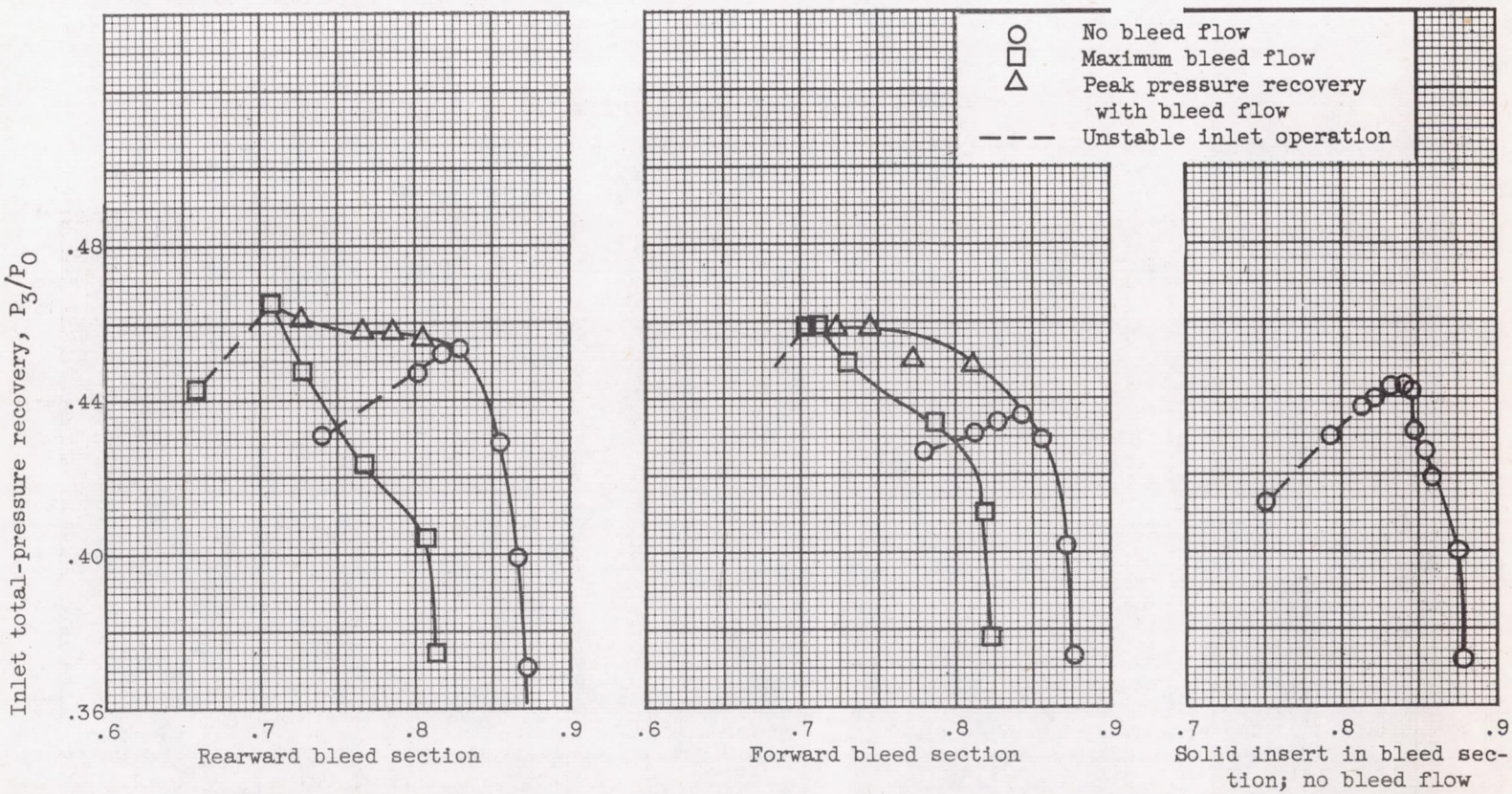

(a) Boundary-layer-removal parameter, h/δ, 0.262.

Figure 11. - Inlet performance with several centerbody bleed sections. 30° Wedge boundary-layer removal.

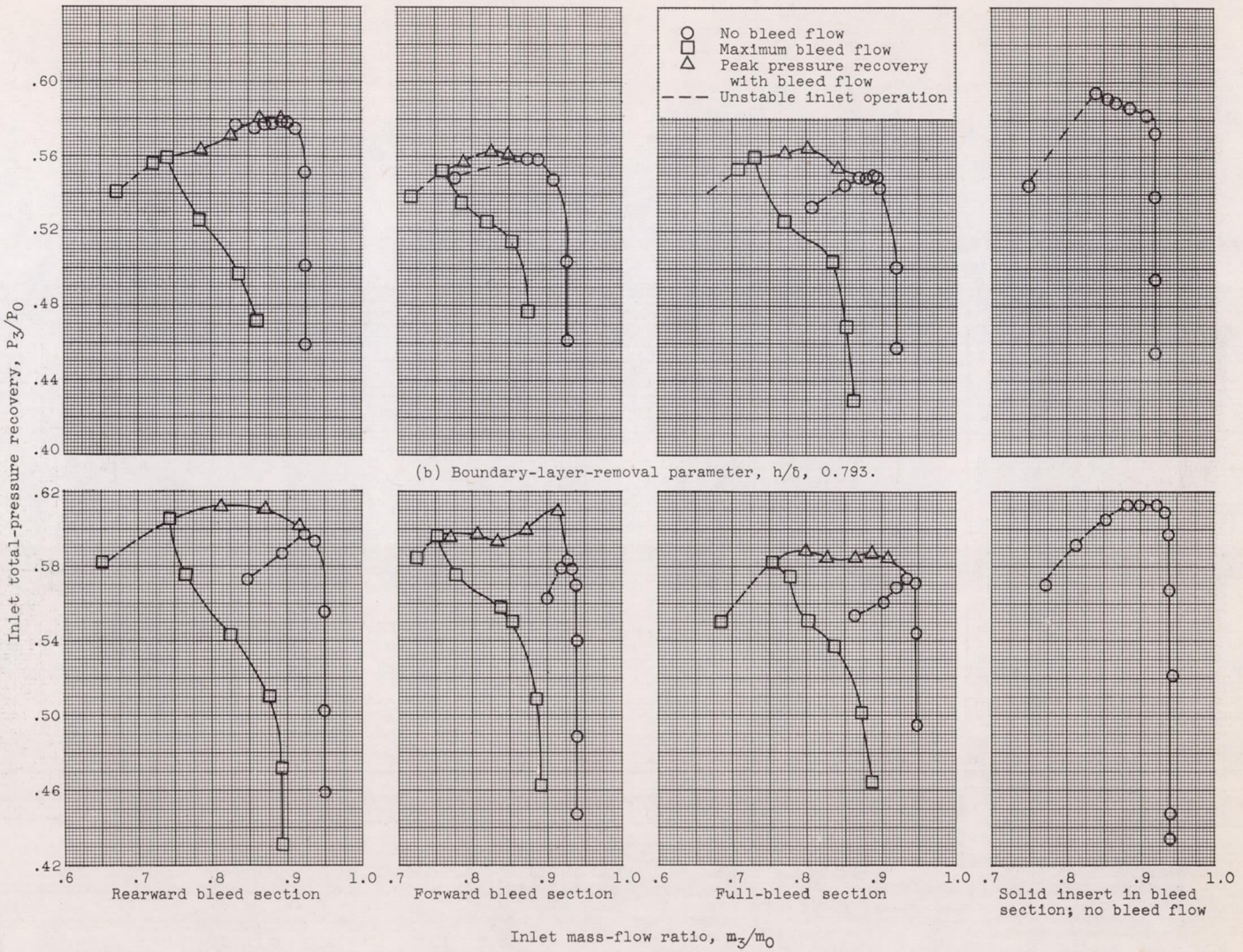

(b) Boundary-layer-removal parameter, h/δ, 0.793.

(c) Boundary-layer-removal parameter, h/δ, 1.055.

Figure 11. - Concluded. Inlet performance with several centerbody bleed sections. 30° Wedge boundary-layer removal.

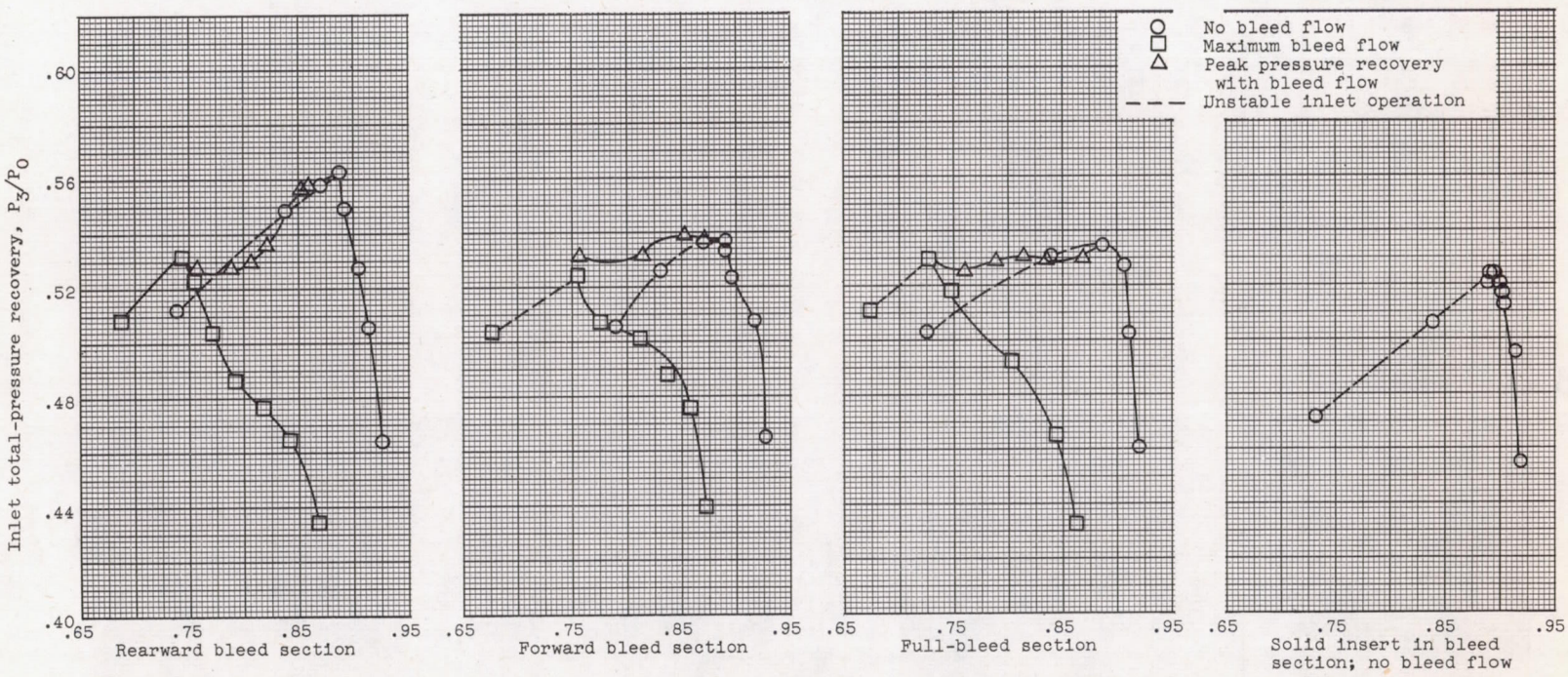

(a) Boundary-layer-removal parameter, h/δ, 0.494.

Figure 12. - Inlet performance with several centerbody bleed sections. 50° Wedge boundary-layer removal.

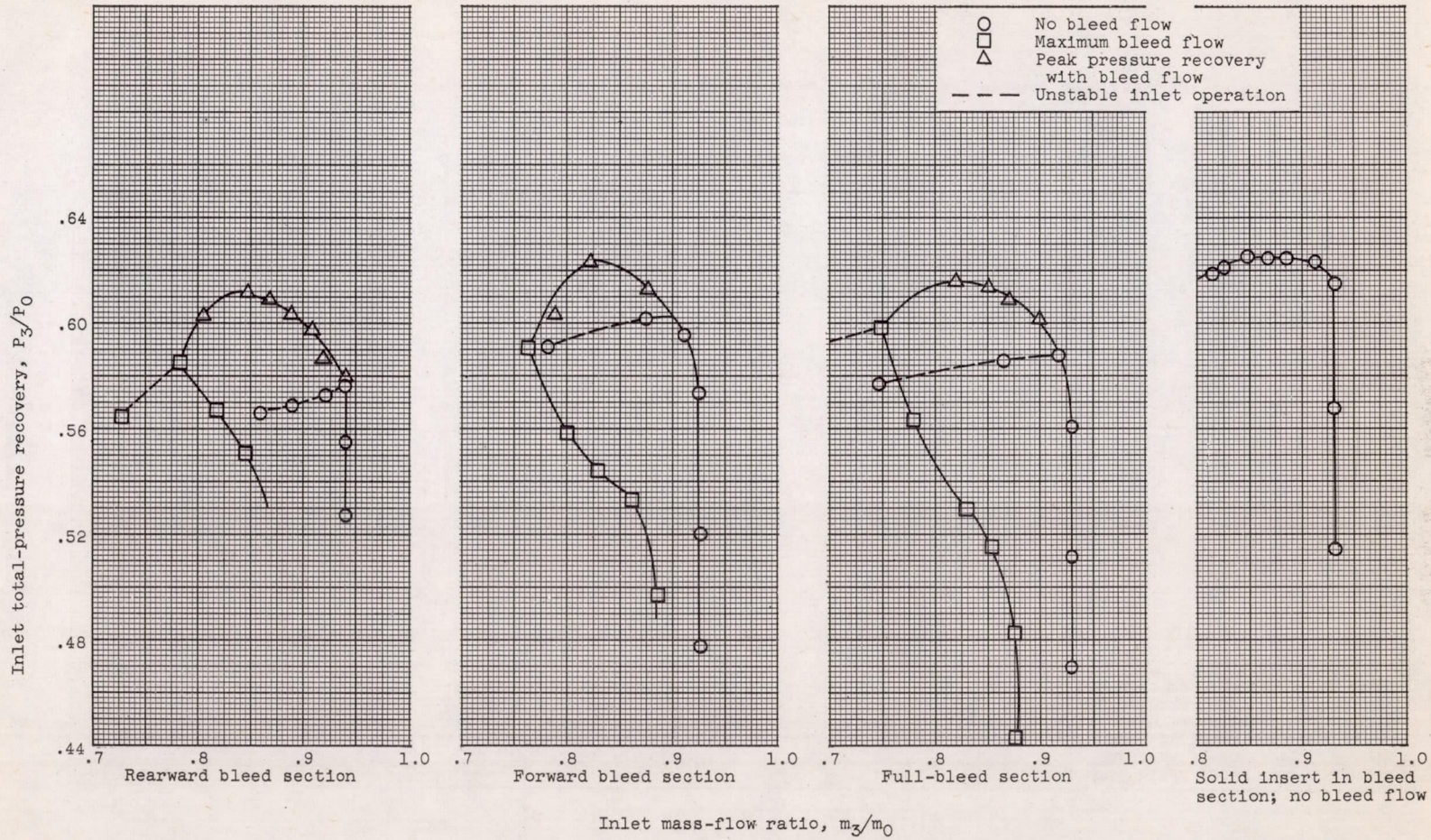

(b) Boundary-layer-removal parameter, h/δ, 0.793.

Figure 12. - Continued. Inlet performance with several centerbody bleed sections. 50° Wedge boundary-layer removal.

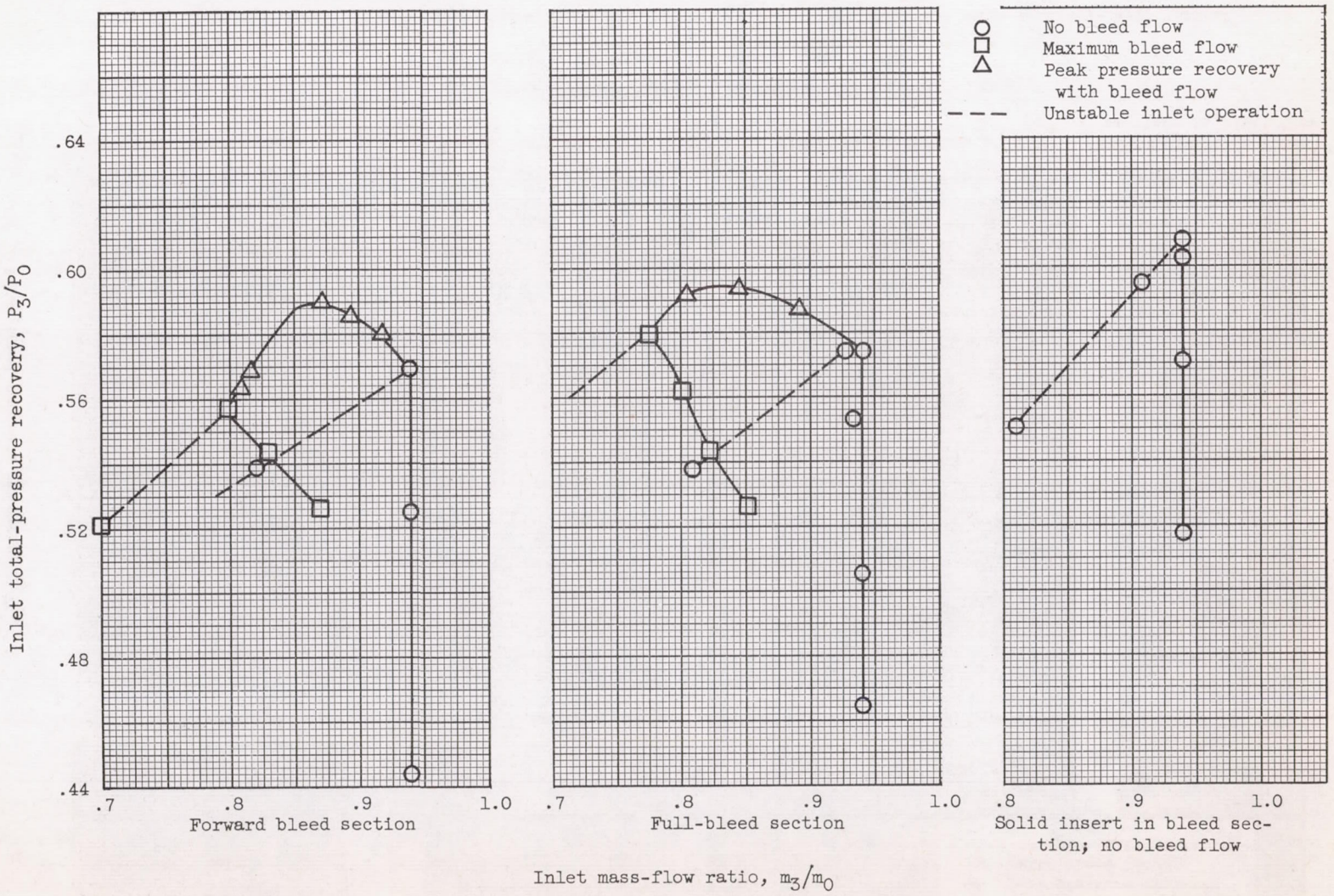

(c) Boundary-layer-removal parameter, h/δ, 1.055.

Figure 12. - Continued. Inlet performance with several centerbody bleed sections. 50° Wedge boundary-layer removal.

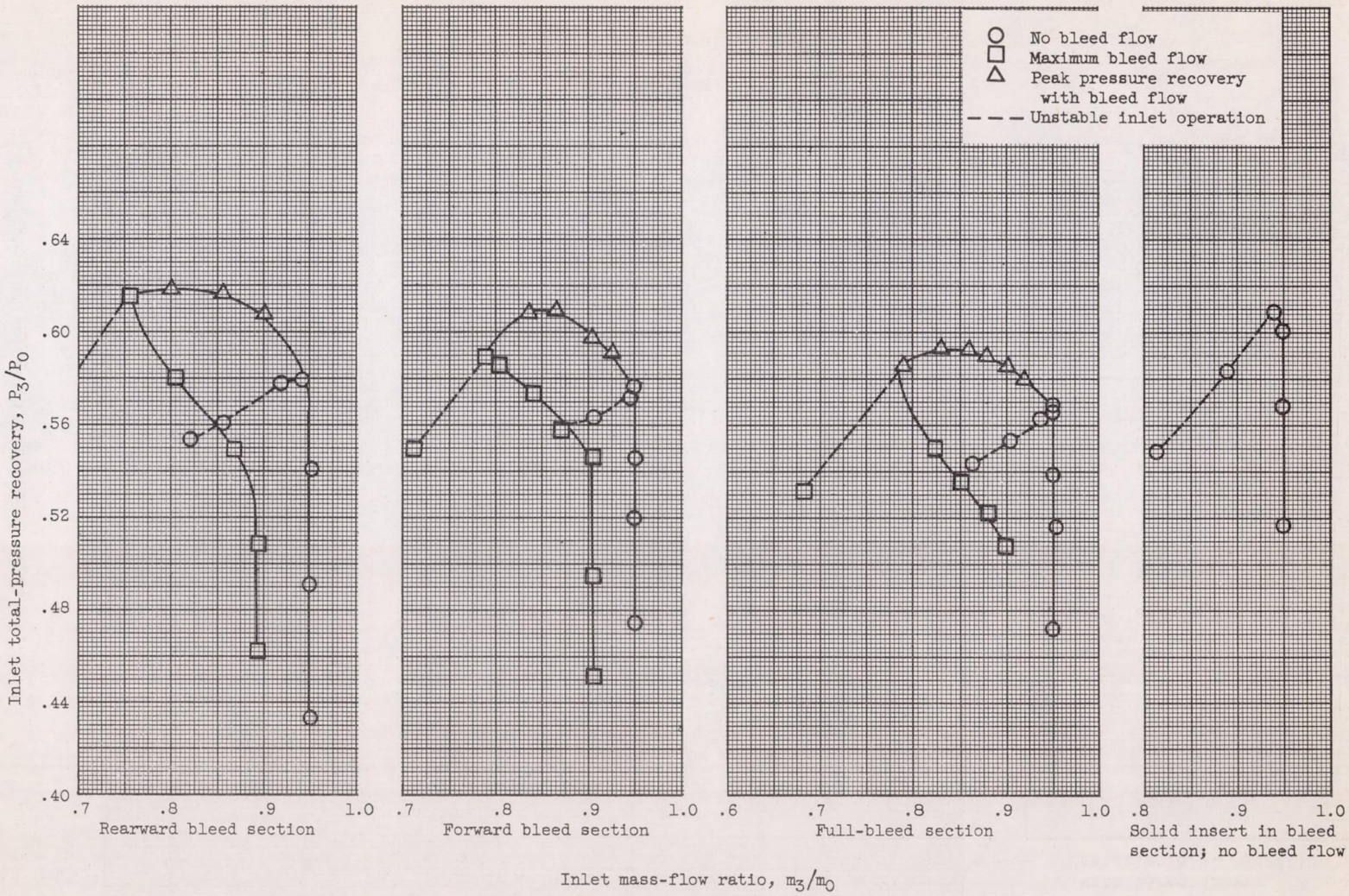

(d) Boundary-layer-removal parameter, h/δ, 1.286.

Figure 12. - Concluded. Inlet performance with several centerbody bleed sections. 50° Wedge boundary-layer removal.

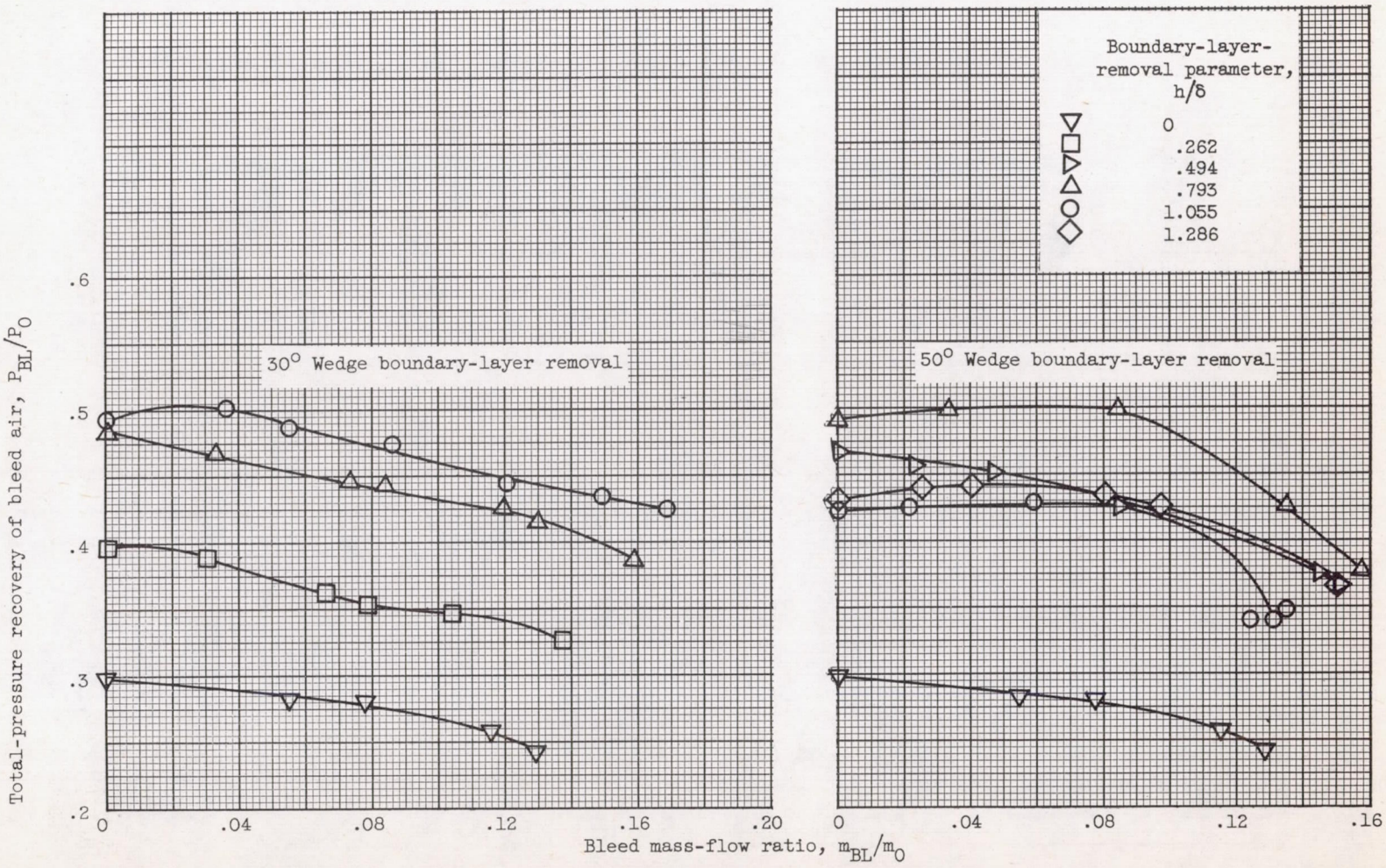

(a) Centerbody bleed sections.

Figure 13. - Bleed pressure recovery.

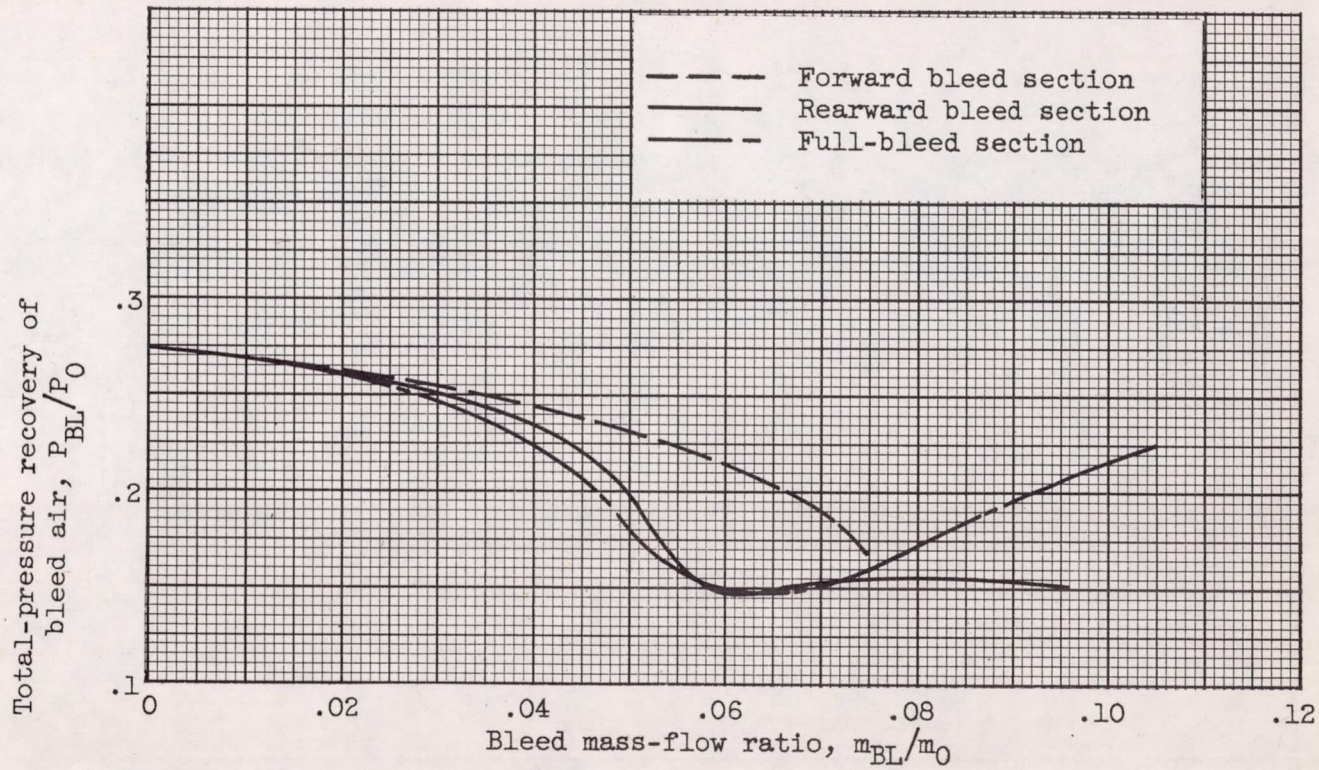

(b) Floor bleed sections. Boundary-layer-removal parameter, h/δ, 0.

Figure 13. - Concluded. Bleed pressure recovery.

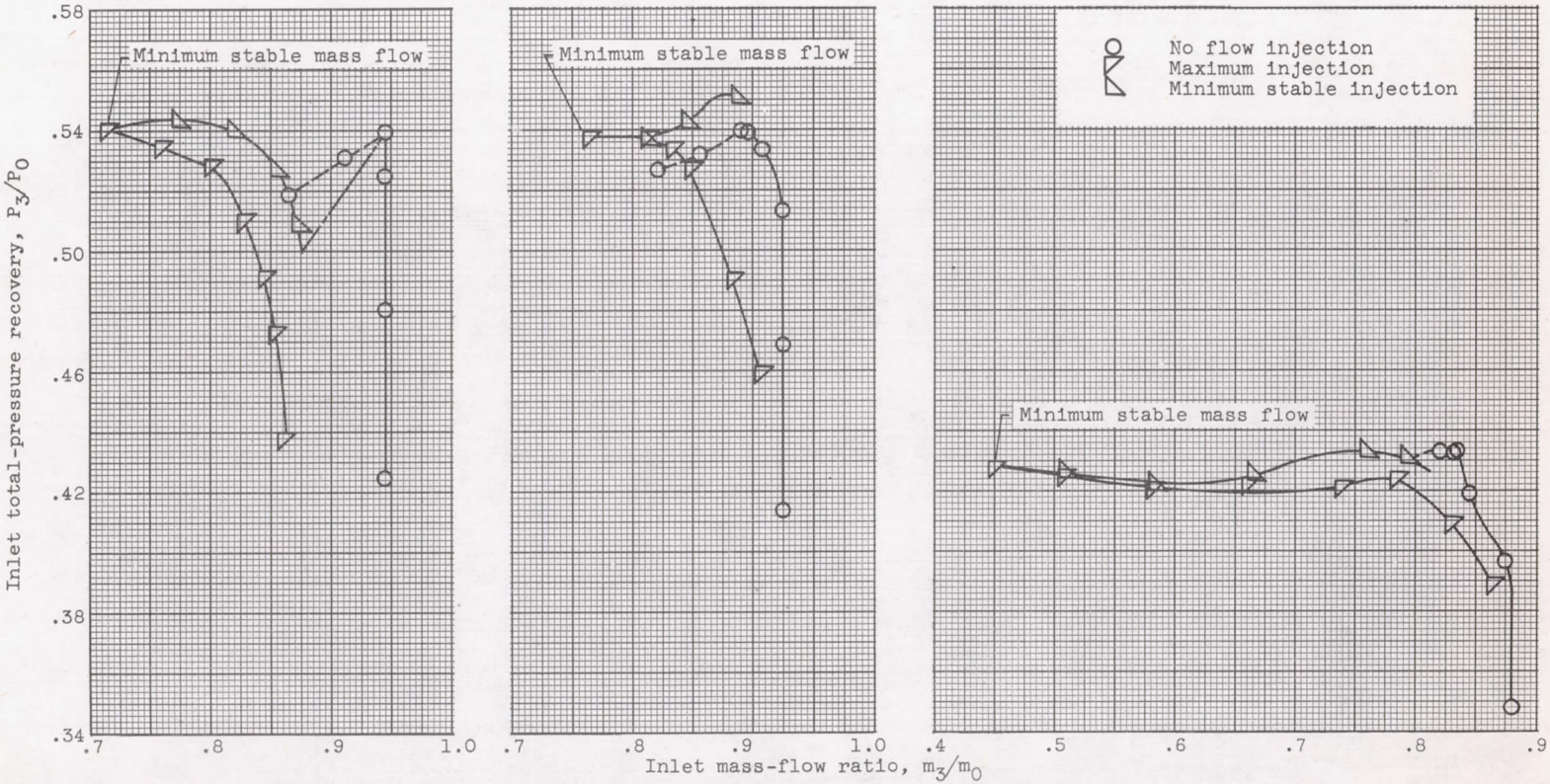

(a) Boundary-layer-removal parameter, h/δ, 1.055. Spike gap, 0.010 inch.

(b) Boundary-layer-removal parameter, h/δ, 0.793. Spike gap, 0.015 inch.

(c) Boundary-layer-removal parameter, h/δ, 0.262. Spike gap, 0.025 inch.

Figure 14. - Effect of flow injection along second cone compression surface. 30° Wedge boundary-layer-removal configuration.

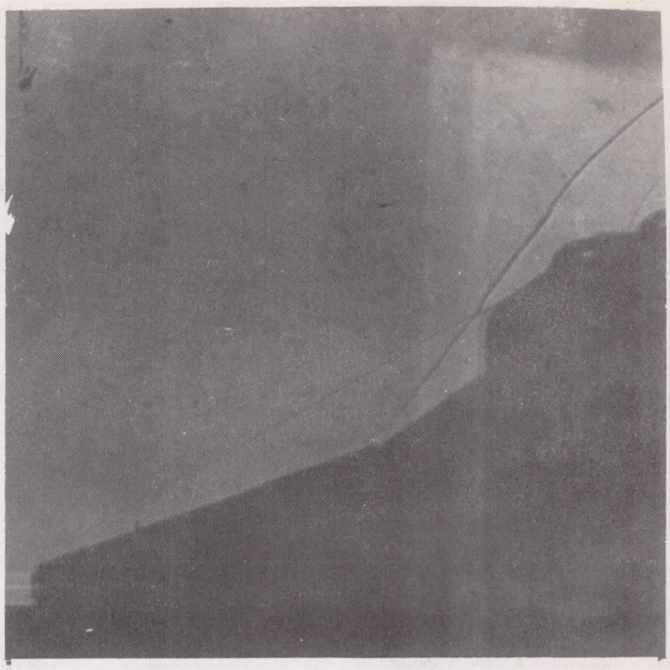

(a) Supercritical inlet operation. No injection.

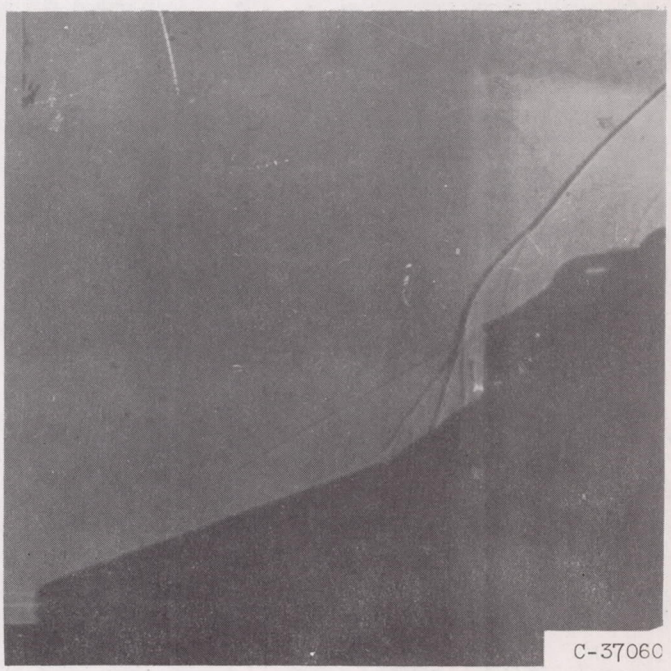

(b) Subcritical stable operation. Flow injection.

Figure 15. - Shadowgraph pictures of flow in region of inlet.

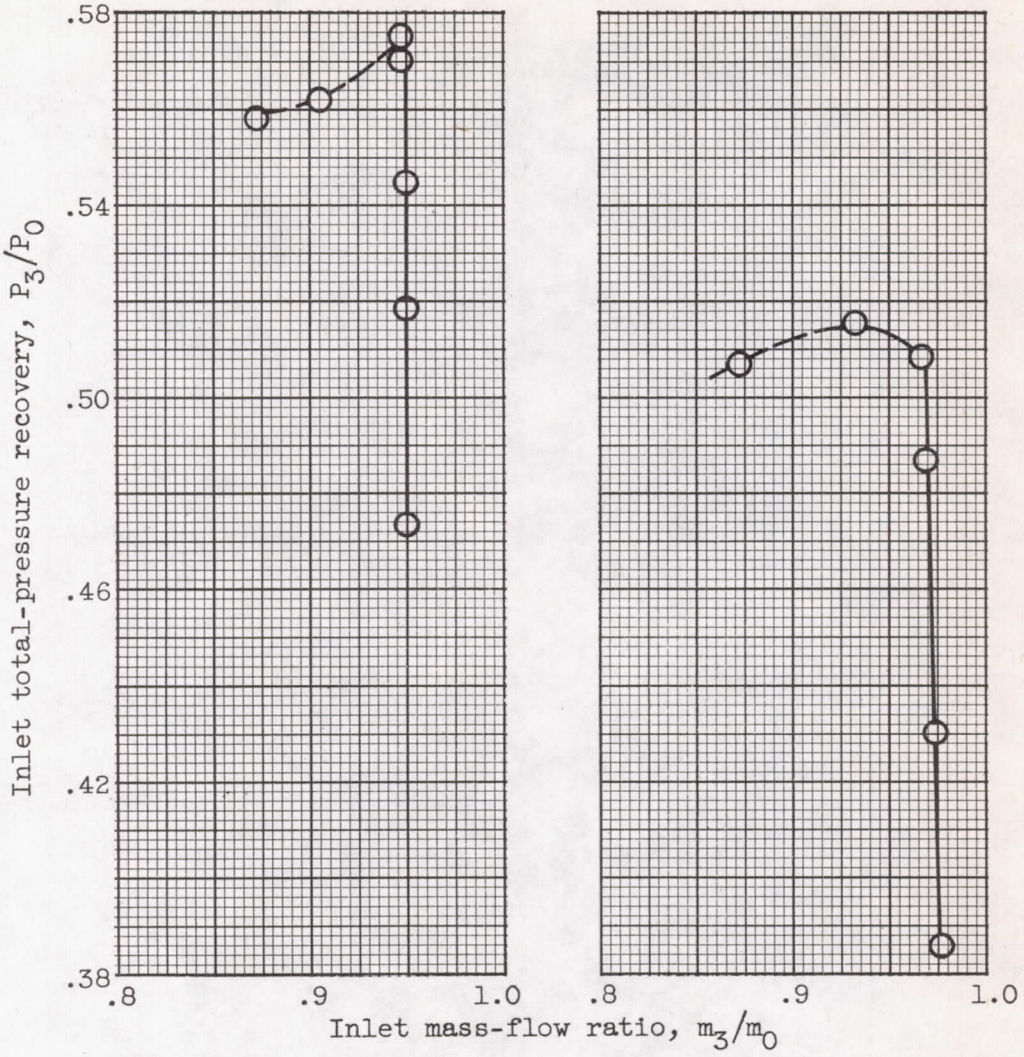

(a) Original spike tip.

(b) Two-piece spike tip with gap closed.

Figure 16. - Effect of oblique-shock location on inlet performance. 50° Wedge boundary-layer removal. Boundary-layer-removal parameter, h/δ, 1.286.

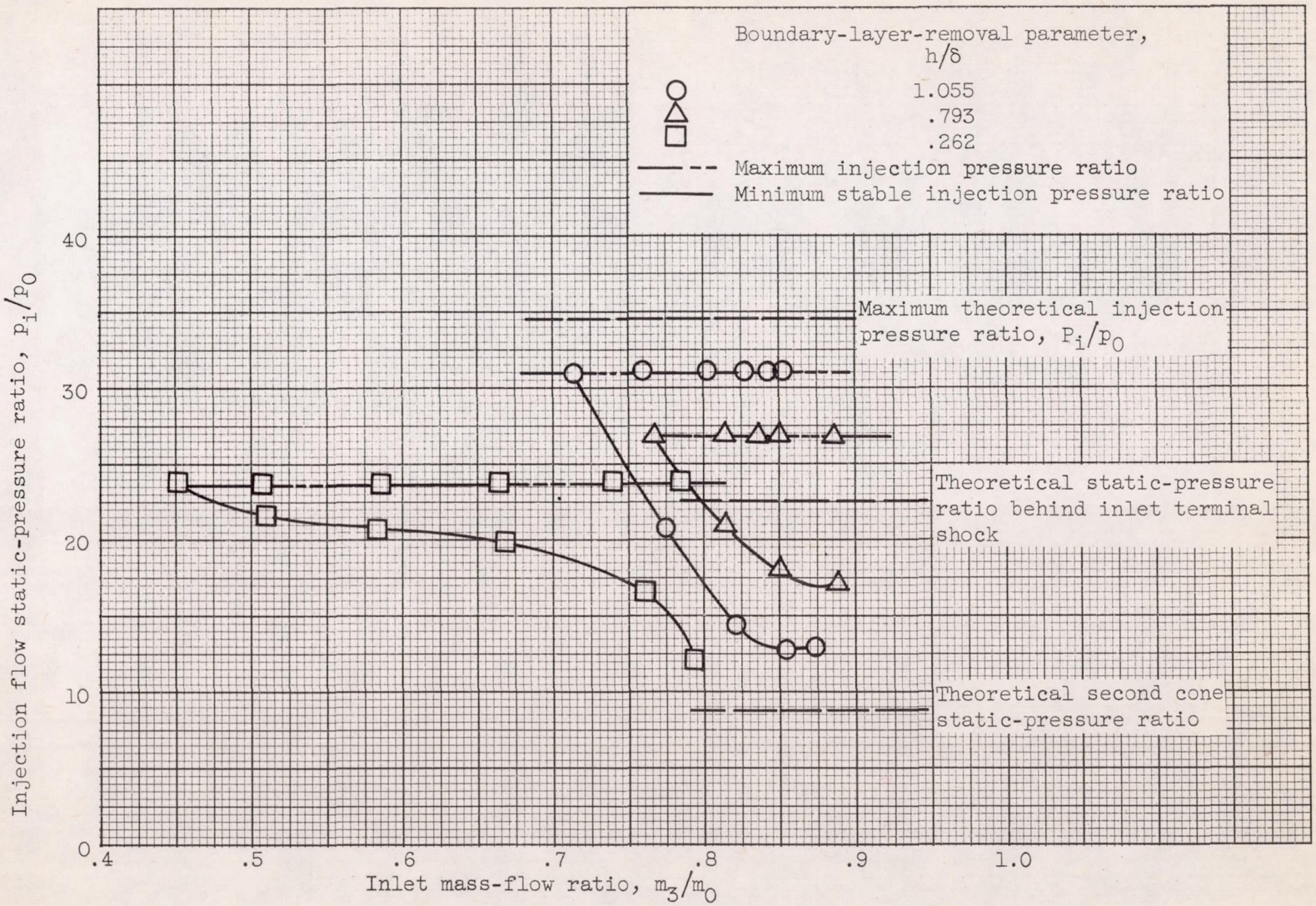

Figure 17. - Pressure ratios for injection air.